

1. Regarding the discussions of the size distributions of  $\text{NO}^+$  and  $\text{NO}_2^+$  ions. It is good the authors have clarified that this is in fact UMR  $m/z$  30 and  $m/z$  46. Consequently, all denotations of those should be changed to  $m/z$  30 and  $m/z$  46 as  $\text{NO}_x^+$  ions should only be used to indicate HR-resolved ions.

However, the discussions/conclusions regarding those size distributions are still a bit under-supported/overstated. While it is stated that  $<10\%$  of those ions were from  $\text{CH}_2\text{O}_x^+$  ions, on average for the HR-MS data, there are 3 reasons that does not suffice along to then go on and make a strong argument that the size-dependent trends in  $m/z$ 30 /  $m/z$ 46 demonstrated organic nitrates dominate at small sizes and are not present at large sizes:

1) The bulk MS data may be dominated by concentrations at larger sizes, thus the  $\text{CH}_2\text{O}^+$  ions may in fact comprise much larger fractions than  $10\%$  compared to either  $\text{NO}_x^+$  ion at the smaller sizes. In fact, for biogenic SOA, it would be surprising if that were not the case. See published spectra of biogenic SOA. For example, in a comparison of UMR and HR nitrate quantification, Fry et al. [2018] showed that on average for a biogenically-influenced region,  $\text{CH}_2\text{O}^+$  was half of the signal at  $m/z$  30. The author could estimate some rough upper limits that the presence of interfering ions could have on the actual  $\text{NO}_x$  ratio at lower sizes. At minimum, this aspect should be acknowledged.

2) The average contributions shown in Fig. S10 as HR spectra, are season averages. It is not clear to a reader if they are representative of the nighttime periods of interest. An analysis using the time-dependent relative contributions could have been more useful.

3) Just because the contribution to nitrate at lower sizes appears to be more from organic nitrates, does not mean they are not present at larger sizes. There seems to be some faulty logic there. This was the reason I suggested in the past review to calculate size distributions of organic and inorganic rather than only framing the discussions in terms of the inorganic/organic relative apportionment which is less relevant to the scientific arguments being made in this paper about organic nitrate production. Maybe the inorganic nitrate is just less present at smaller sizes.

#### **REPLY:**

We have changed all relevant  $\text{NO}^+/\text{NO}_2^+$  to  $m/z$  30/ $m/z$  46 in section 3.3. And the time variations of contributions of  $\text{CH}_2\text{O}^+$  in  $m/z$  30 and  $\text{CH}_2\text{O}_2^+$  in  $m/z$  46 in the HR data of  $\text{PM}_{10}$  for the four seasons are shown in Figure S10. We further checked the size distributions of  $m/z$  30/ $m/z$  46 ratio under the highest ( $>15\%$ ) and lowest interferences ( $<5\%$ )  $\text{CH}_2\text{O}_x^+$  interferences in spring, summer and autumn (Figure S12), the results show that  $m/z$  30/ $m/z$  46 variation patterns are not significantly affected by the interferences of  $\text{CH}_2\text{O}_x^+$ . Additionally, we used the size distributions of the  $m/z$  30/ $m/z$  46 ratio to separate the size distributions of inorganic and organic nitrates, as shown in Figure S13 according to the suggestion. The statements about organic nitrates are not present at larger sizes are deleted and we only address that organic nitrates were relatively more concentrated at small sizes compared to inorganic nitrates. The relevant changes in section 3.3 are as follow:

“In this section, we attempt to use the  $\text{NO}^+/\text{NO}_2^+$  ratio as an indicator to investigate the size distribution characteristics of organic nitrates. Unfortunately, due to the lack of HR-PToF data, our analyses used the UMR-PToF data of  $m/z$  30 and 46, which might contain the interferences of  $\text{CH}_2\text{O}_x^+$  (Fry et al., 2018). In our case, the time variations of contributions of  $\text{CH}_2\text{O}^+$  in  $m/z$  30 and  $\text{CH}_2\text{O}_2^+$  in  $m/z$  46 in the HR data of  $\text{PM}_{10}$  for the four seasons are shown in Figure S10. For all the four seasons, the average contributions of  $\text{CH}_2\text{O}_x^+$  in  $m/z$  30 and 46 in the HR data of  $\text{PM}_{10}$  were less than  $10\%$ , suggesting that the  $m/z$  30/ $m/z$  46 ratio could mostly represent the  $\text{NO}^+/\text{NO}_2^+$  ratio. The average size distributions of  $m/z$  30 and  $m/z$  46 for the four seasons are shown in Figure S11, and Figure 4a shows the average size

distributions of different aerosol species and the m/z 30/m/z 46 ratio in the four seasons. It is clearly found that the m/z 30/m/z 46 ratio exhibited a decreasing trend in spring, summer and autumn, while it kept constant in winter, similar to the value of  $R_{\text{NH}_4\text{NO}_3}$  (red dotted line in Figure 4a). In addition, in spring, summer and autumn, the lowest values of the m/z 30/m/z 46 ratio, occurring at  $\sim 1 \mu\text{m}$ , were approximate to the corresponding seasonal values of  $R_{\text{NH}_4\text{NO}_3}$ . It should be noted that the similar size distribution patterns of the m/z 30/m/z 46 ratio under the highest interferences (>15%) and lowest interferences (<5%) of  $\text{CH}_2\text{O}_x^+$ , indicated by the HR data of  $\text{PM}_{10}$ , for spring, summer and autumn (Figure S12) imply that the size distribution patterns of the m/z 30/m/z 46 ratio were not affected significantly by the interferences of  $\text{CH}_2\text{O}_x^+$ . We also used the size distributions of the m/z 30/m/z 46 ratio to separate the size distributions of inorganic and organic nitrates, as shown in Figure S13, and the results indicate that organic nitrates were relatively more concentrated at small sizes compared to inorganic nitrates.”

2. SOA yield is dependent on organic aerosol mass. When using the SOA yields in literature to estimate SOA from VOC+NO<sub>3</sub> (Table 3), please ensure that the yields used are from laboratory experiments that covered the relevant range of aerosol mass in the field campaigns. Please clarify this in the revised manuscript.

**REPLY:**

We have double checked the literature to make sure the chamber conditions to obtain the yields covered the range of aerosol mass loading in the spring campaign. The relevant clarification is added in the revised manuscript.

3. There are a number of grammatical mistakes / typos, e.g., line 303 should be "associated with", etc. Please correct them.

**REPLY:**

We have corrected them.

## A list of all relevant changes

1. Line 197-202: Changed to “Unfortunately, due to the lack of HR-PTof data, our analyses used the UMR-PTof data of  $m/z$  30 and 46, which might contain the interferences of  $\text{CH}_2\text{O}_x^+$  (Fry et al., 2018). In our case, the time variations of contributions of  $\text{CH}_2\text{O}^+$  in  $m/z$  30 and  $\text{CH}_2\text{O}_2^+$  in  $m/z$  46 in the HR data of  $\text{PM}_{10}$  for the four seasons are shown in Figure S10. For all the four seasons, the average contributions of  $\text{CH}_2\text{O}_x^+$  in  $m/z$  30 and 46 in the HR data of  $\text{PM}_{10}$  were less than 10%, suggesting that the  $m/z$  30/ $m/z$  46 ratio could mostly represent the  $\text{NO}^+/\text{NO}_2^+$  ratio. The average size distributions of  $m/z$  30 and  $m/z$  46 for the four seasons are shown in Figure S11”.
2. Line 206-211: Added “It should be noted that the similar size distribution patterns of the  $m/z$  30/ $m/z$  46 ratio under the highest interferences (>15%) and lowest interferences (<5%) of  $\text{CH}_2\text{O}_x^+$ , indicated by the HR data of  $\text{PM}_{10}$ , for spring, summer and autumn (Figure S12) imply that the size distribution patterns of the  $m/z$  30/ $m/z$  46 ratio were not affected significantly by the interferences of  $\text{CH}_2\text{O}_x^+$ . We also used the size distributions of the  $m/z$  30/ $m/z$  46 ratio to separate the size distributions of inorganic and organic nitrates, as shown in Figure S13, and the results indicate that organic nitrates were relatively more concentrated at small sizes compared to inorganic nitrates”.
3. Line 249-250: Added “where the chamber conditions to obtain the yields covered the range of aerosol mass loading in the spring campaign”.
4. Line 305: Changed to “associated”.
5. Line 383-387: Added “Fry, J. L., Brown, S. S., Middlebrook, A. M., Edwards, P. M., Campuzano-Jost, P., Day, D. A., Jimenez, J. L., Allen, H. M., Ryerson, T. B., Pollack, I., Graus, M., Warneke, C., de Gouw, J. A., Brock, C. A., Gilman, J., Lerner, B. M., Dubé, W. P., Liao, J., and Welti, A.: Secondary organic aerosol (SOA) yields from  $\text{NO}_3$  radical + isoprene based on nighttime aircraft power plant plume transects, *Atmos. Chem. Phys.*, 18, 11663-11682, <https://doi.org/10.5194/acp-18-11663-2018>, 2018”.
6. Line 333-335: Added “Author contributions. Xiao-Feng Huang designed the research. Kuangyou Yu and Qiao Zhu conducted data analysis and wrote the paper. Ke Du contributed to modelling and writing”.

# Characterization of nighttime formation of particulate organic nitrates based on high-resolution aerosol mass spectrometry in an urban atmosphere in China

Kuangyou Yu<sup>1,2,\*</sup>, Qiao Zhu<sup>1,\*</sup>, Ke Du<sup>2</sup>, Xiao-Feng Huang<sup>1</sup>

<sup>1</sup>Key Laboratory for Urban Habitat Environmental Science and Technology, School of Environment and Energy, Peking University Shenzhen Graduate School, Shenzhen, 518055, China.

<sup>2</sup>Department of Mechanical and Manufacturing Engineering, University of Calgary, Calgary, Canada.

\* Authors have equal contribution.

**Abstract.** Organic nitrates are important atmospheric species that significantly affect the cycling of NO<sub>x</sub> and ozone production. However, characterization of particulate organic nitrates and their sources in polluted atmosphere is a big challenge and has not been comprehensively studied in Asia. In this study, an Aerodyne high-resolution time-of-flight aerosol mass spectrometer (HR-ToF-AMS) was deployed at an urban site in China from 2015 to 2016 to characterize particulate organic nitrates in total nitrates with high time resolution. Based on the cross validation of two different data processing methods, organic nitrates were effectively quantified to contribute a notable fraction of organic aerosol (OA): 9-21% in spring, 11-25% in summer, 9-20% in autumn, while very small fraction in winter. The good correlation between organic nitrates and fresh secondary organic aerosol (SOA) at night, as well as the diurnal trend of size distribution of organic nitrates, indicated a key role of nighttime local secondary formation of organic nitrates in Shenzhen. Furthermore, theoretical calculations of nighttime SOA production of NO<sub>3</sub> reactions with volatile organic compounds (VOCs) measured during the spring campaign were performed, resulting in three biogenic VOCs ( $\alpha$ -pinene, limonene, and camphene) and one anthropogenic VOC (styrene) identified as the possible key VOC precursors for particulate organic nitrates. The comparison with similar studies in the literature implied that nighttime particulate organic nitrates formation is highly relevant with NO<sub>x</sub> levels. This study proposes that unlike the documented cases in the United States and Europe, modeling nighttime particulate organic nitrate formation in China should incorporate not only biogenic VOCs but also anthropogenic VOCs for urban air pollution, which needs the support of relevant smog chamber studies in the future.

---

Correspondence to: X.-F. Huang ([huangxf@pku.edu.cn](mailto:huangxf@pku.edu.cn))

## 29 1. Introduction

30 Organic nitrates (ON) in aerosols have an important impact on the fate of NO<sub>x</sub> and ozone production (Lelieveld et al., 2016),  
31 which can be formed in a minor channel of the reaction between peroxy radicals and NO (R1 and R2) (usually, an increased  
32 fraction of this reaction leads to the formation of alkoxy radicals and NO<sub>2</sub> (R3)) or via the NO<sub>3</sub>-induced oxidation of unsaturated  
33 hydrocarbons (R4). Even though some recent studies have suggested that the formation of organic nitrates from peroxy radicals  
34 and NO may play a larger role than previously recognized (Teng et al., 2015, 2017), yields of organic nitrates via NO<sub>3</sub> reacting  
35 with alkenes are generally much higher (Fry et al., 2009; Ayres et al., 2015; Boyd et al., 2015, 2017).



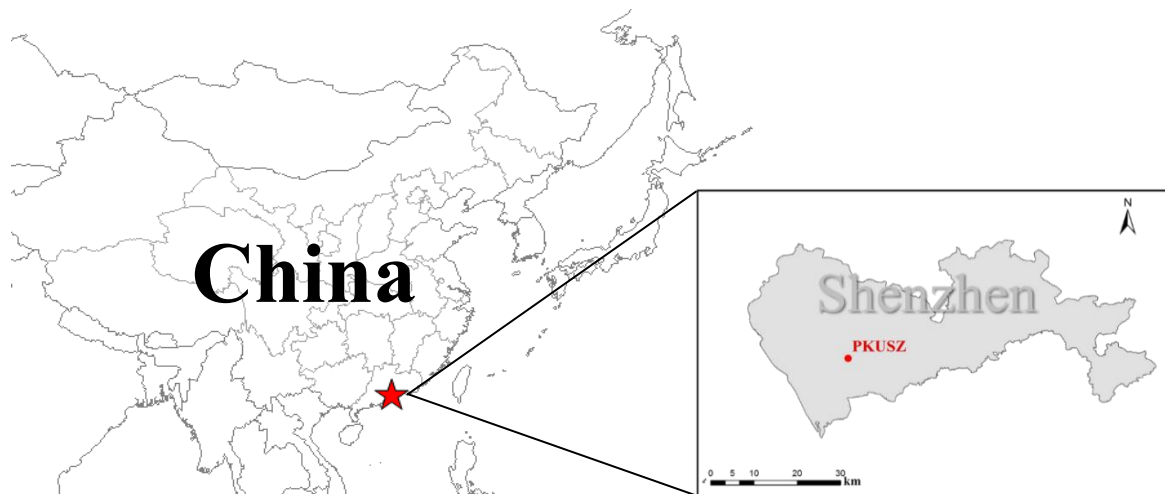
40 Several methods have been developed to directly measure total organic nitrates (gas + particle) in the real atmosphere. For  
41 example, Rollins et al. (2012) used a thermal-dissociation laser-induced fluorescence technique (TD-LIF) to observe organic  
42 nitrates in the United States; Sobanski et al. (2017) measured organic nitrates in Germany using the thermal dissociation cavity  
43 ring-down spectroscopy (TD-CRDS). Field and laboratory studies around the world indicated that particulate organic nitrates  
44 could contribute a large portion of secondary organic aerosol (SOA) (Rollins et al., 2012; Xu et al., 2015a; Fry et al., 2013;  
45 Ayres et al., 2015; Boyd et al., 2015; Lee et al., 2016). Recently, researchers have proposed some estimation methods for  
46 particle-phase organic nitrates based on aerosol mass spectrometry (AMS) with high time resolution (Farmer et al., 2010; Hao  
47 et al., 2014; Xu et al., 2015a, 2015b). Ng et al. (2017) reviewed the nitrate radical chemistry and the abundance of particulate  
48 organic nitrates in the United States and Europe, and further concluded that particulate organic nitrates are formed substantially  
49 via NO<sub>3</sub>+BVOC chemistry, which plays an important role in SOA formation. Unfortunately, relevant Chinese datasets are  
50 scarce yet and not included in this review. This was because (1) the contributions of organic nitrates in SOA and total nitrates  
51 in Chinese atmosphere remain poorly understood; (2) the anthropogenic and biogenic precursor emissions in China are  
52 significantly different from those in the United States and Europe, and thus cannot be easily estimated. To our best knowledge,  
53 few studies have investigated the concentrations and formation pathways of particulate organic nitrates in China. Xu et al.  
54 (2017) estimated the mass concentration of organic nitrogen in Beijing using AMS, but in this study they ignored the  
55 contribution of NO<sub>x</sub><sup>+</sup> family, which are the major fragments of organic nitrates.

56 Shenzhen is a megacity of China in a subtropical region, where NO<sub>x</sub> involved photochemical reactions are very active, given  
57 considerable biogenic and anthropogenic VOC emissions (Zhang et al., 2008). To assess the evolution of particulate organic  
58 nitrates in a polluted urban atmosphere, we deployed an Aerodyne high-resolution time-of-flight aerosol mass spectrometer  
59 (HR-ToF-AMS) and other instruments in Shenzhen from 2015 to 2016 in this study. Organic nitrates and their contributions  
60 to OA in different seasons were estimated by different methods using the HR-ToF-AMS datasets, based on which, the  
61 secondary formation pathway of particulate organic nitrates in Shenzhen was further explored.

## 62 2. Experiment methods

### 63 2.1 Sampling site and period

64 The sampling site (22.6°N, 113.9°E) was on the roof (20 m above ground) of an academic building on the campus of Peking  
65 University Shenzhen Graduate School (PKUSZ), which is located in the western urban area in Shenzhen (Figure 1). This site  
66 is mostly surrounded by subtropical plants without significant anthropogenic emission sources nearby, except a local road that  
67 is ~100 m from the site. In this study, we used the statistical data from the Meteorological Bureau of Shenzhen Municipality  
68 (<http://www.szmb.gov.cn/site/szmb/Esztq/index.html>) as the reference data to determine the sampling periods for four  
69 different seasons during 2015-2016, as shown in Table 1.



70

71

**Figure 1.** The location of the sampling site.

72 **Table 1.** Meteorological conditions, PM<sub>1</sub> species concentrations and relevant parameters for different sampling periods in  
73 Shenzhen.

	Sampling period	4.1-4.30, 2016	8.1-8.31, 2015	11.4-11.30, 2015	1.21-2.3, 2016
		Spring	Summer	Autumn	Winter
<b>Meteorology</b>	T (°C)	24.5±2.5	29.0±3.0	23.6±3.7	10.7±4.7
	RH (%)	78.0±12.7	71.2±17.5	68.2±15.8	75.4±18.7
	WS (m s <sup>-1</sup> )	1.4±0.8	1.0±0.7	1.2±0.7	1.5±0.8
<b>Species</b>	Org	4.3±3.2	10.0±6.9	7.8±5.9	5.1±3.5
	SO <sub>4</sub> <sup>2-</sup>	3.2±1.8	5.8±3.3	2.3±1.5	1.9±1.2
	Total NO <sub>3</sub> <sup>-</sup>	0.96±1.4	0.91±0.90	1.3±1.4	1.6±1.0

$(\mu\text{g m}^{-3})$	$\text{NH}_4^+$	1.4±0.8	2.0±1.1	1.1±0.8	1.2±0.6
	$\text{Cl}^-$	0.14±0.19	0.03±0.05	0.22±0.36	0.64±0.85
	BC	1.9±2.1	2.4±1.6	3.5±2.6	2.4±1.5
	Total	12.0±8.9	15.1±13.8	11.8±9.5	12.2±7.2
<b>ON relevant</b>	$R_{\text{NH}_4\text{NO}_3}$	2.80	3.20	3.32	3.48
	$R_{\text{obs}}$	3.74	6.14	4.30	3.55
<b>parameters</b>	Fraction of positive numbers of $R_{\text{obs}} - R_{\text{NH}_4\text{NO}_3}$	99%	99%	84%	47%

## 74 2.2 Instrumentation

### 75 2.2.1 High Resolution Time-of-Flight Aerosol Mass Spectrometer

76 During the sampling periods, chemical composition of non-refractory  $\text{PM}_{10}$  was measured by an Aerodyne HR-ToF-AMS, and  
77 detailed descriptions of this instrument are given in the literature (DeCarlo et al., 2006; Canagaratna et al., 2007). The setup  
78 and operation of the HR-ToF-AMS can be found in our previous publications (Huang et al., 2010, 2012; Zhu et al., 2016). To  
79 remove coarse particles, a  $\text{PM}_{2.5}$  cyclone inlet was installed before the sampling copper tube with a flow rate of  $10 \text{ l min}^{-1}$ .  
80 Before entering the AMS, the sampled air was dried by a nafion dryer (MD-070-12S-4, Perma Pure Inc.) to eliminate the  
81 potential influence of relative humidity on particle collection (Matthew et al., 2008). The ionization efficiency (IE) calibrations  
82 were performed using pure ammonium nitrate every two weeks. The relative ionization efficiencies (RIEs) used in this study  
83 were 1.2 for sulfate, 1.1 for nitrate, 1.3 for chloride, 1.4 for organics and 4.0 for ammonium, respectively (Jimenez et al., 2003).  
84 Composition-dependent collection efficiencies (CEs) were applied to the data according to the method in Middlebrook et al.  
85 (2012). The instrument was operated at two ion optical modes with a cycle of 4 min, including 2 min for the mass-sensitive  
86 V-mode and 2 min for the high mass resolution W-mode. The HR-ToF-AMS data analysis was performed using the software  
87 SQUIRREL (version 1.57) and PIKA (version 1.16) written in Igor Pro 6.37 (Wave Metrics Inc.)  
88 (<http://cires1.colorado.edu/jimenezgroup/ToFAMSResources/ToFSoftware/index.html>).

### 89 2.2.2 Other co-located instruments

90 In addition to the HR-ToF-AMS, other relevant instruments were deployed at the same sampling site. An aethalometer (AE-  
91 31, Magee) was used for measurement of refractory black carbon (BC) with a resolution of 5 min. An SMPS system (3775  
92 CPC and 3080 DMA, TSI Inc.) was used to obtain the particle number size distribution in 15–615 nm (mobility diameter) with  
93 a time resolution of 5 min. Ozone and  $\text{NO}_x$  were measured by a 49i ozone analyzer and a 42i nitrogen oxide analyzer (Thermo  
94 Scientific), respectively. In the spring campaign, ambient VOC concentrations were also measured using an on-line VOC  
95 monitoring system (TH-300B, Tianhong Corp.), including an ultralow-temperature preconcentration cold trap and an

96 automated in-situ gas chromatograph (Agilent 7820A) equipped with a mass spectrometer (Agilent 5977E). The system had  
97 both a flame ionization detector (FID) gas channel for C2–C5 hydrocarbons and a mass spectrometer (MS) gas channel for  
98 C5–C12 hydrocarbons, halohydrocarbons and oxygenated VOCs. A complete working cycle of the system was one hour and  
99 included six steps: sample collection, freeze-trapping, thermal desorption, GC-FID/MS analysis, heating and anti-blowing  
100 purification. The sample collection time was 5 min. The sampling flow speed was 60 ml min<sup>-1</sup>. The anti-blowing flow speed  
101 was 200 ml min<sup>-1</sup>. The calibration of over 100 VOCs was performed using mixed standard gas before and after the campaign.  
102 Detection limits for most compounds were near 5 pptv. More description of this instrument can be found in Wang et al. (2014).

### 103 2.3 Organic nitrates estimation methods

104 In this study, we used two independent methods to estimate particulate organic nitrates based on the AMS data, following the  
105 approaches in Xu et al. (2015b). The first method is based on the NO<sup>+</sup>/NO<sub>2</sub><sup>+</sup> ratio (NO<sub>X</sub><sup>+</sup> ratio) in the HR-AMS spectrum. Due  
106 to the very different NO<sub>X</sub><sup>+</sup> ratios of organic nitrates and inorganic nitrate (i.e., R<sub>ON</sub> and R<sub>NH<sub>4</sub>NO<sub>3</sub></sub>, respectively) (Farmer et al.,  
107 2010; Boyd et al., 2015; Fry et al., 2008; Bruns et al., 2010), the NO<sub>2</sub><sup>+</sup> and NO<sup>+</sup> concentrations of organic nitrates (NO<sub>2,ON</sub> and  
108 NO<sub>ON</sub>) can be quantified with the HR-AMS data via Eqs. (1) and (2), respectively (Farmer et al., 2010):

$$109 \quad NO_{2,ON}^+ = \frac{NO_{2,obs}^+ \times (R_{obs} - R_{NH_4NO_3})}{R_{ON} - R_{NH_4NO_3}} \quad (1)$$

$$110 \quad NO_{ON}^+ = R_{ON} \times NO_{2,ON} \quad (2)$$

111 where R<sub>obs</sub> is the NO<sub>X</sub><sup>+</sup> ratio from the observation. The value of R<sub>ON</sub> is difficult to determine because it varies between  
112 instruments and precursor VOCs. However, R<sub>NH<sub>4</sub>NO<sub>3</sub></sub> was determined by IE calibration using pure NH<sub>4</sub>NO<sub>3</sub> every two weeks  
113 for each campaign and the results showed stable values: In spring, the average R<sub>NH<sub>4</sub>NO<sub>3</sub></sub> was 2.66 for the first IE calibration and  
114 2.94 for the second one; in summer, the average R<sub>NH<sub>4</sub>NO</sub> was 3.05 and 3.34 for the first and second IE calibrations, respectively;  
115 in autumn, the average R<sub>NH<sub>4</sub>NO<sub>3</sub></sub> was 3.33 and 3.31 for the first and second IE calibrations, respectively; in winter, the average  
116 R<sub>NH<sub>4</sub>NO<sub>3</sub></sub> was 3.45 and 3.51 for the first and second IE calibrations, respectively. We adopted the R<sub>ON</sub>/R<sub>NH<sub>4</sub>NO<sub>3</sub></sub> estimation range  
117 (from 2.08 to 3.99) for variation of precursor VOCs in the literature to determine R<sub>ON</sub> (Farmer et al., 2010; Boyd et al., 2015;  
118 Bruns et al., 2010; Sato et al., 2010; Xu et al., 2015b), and thus two R<sub>ON</sub> values were calculated for each season to provide the  
119 upper bound (NO<sub>3\_organic\_ratio\_1</sub>) and lower bound (NO<sub>3\_organic\_ratio\_2</sub>) of NO<sub>3,org</sub> mass concentration.

120 The second method is based on the traditional positive matrix factorization (PMF) analysis of HR organic mass spectra, which  
121 resolves different organic factors (Zhang et al., 2011; Ng et al., 2010; Huang et al., 2013). Combined with NO<sup>+</sup> and NO<sub>2</sub><sup>+</sup> ions,  
122 the same analysis of HR organic mass spectra was performed to separate NO<sup>+</sup> and NO<sub>2</sub><sup>+</sup> ions into different organic factors and  
123 an inorganic nitrate factor (Hao et al., 2014; Xu et al., 2015b). The PMF analysis procedures in this study can be found in our  
124 previous publications (Huang et al., 2010; Zhu et al., 2016; He et al., 2011), resulting in three organic factors and one inorganic  
125 factor in spring, summer and autumn: a hydrocarbon-like OA (HOA) characterized by C<sub>n</sub>H<sub>2n+1</sub><sup>+</sup> and C<sub>n</sub>H<sub>2n-1</sub><sup>+</sup> and O/C of 0.11  
126 to 0.18, a less-oxidized oxygenated OA (LO-OOA) characterized by C<sub>x</sub>H<sub>y</sub>O<sub>z</sub><sup>+</sup> especially C<sub>2</sub>H<sub>3</sub>O<sup>+</sup> and O/C of 0.28 to 0.70, a  
127 more-oxidized oxygenated OA (MO-OOA) also characterized by C<sub>x</sub>H<sub>y</sub>O<sub>z</sub><sup>+</sup> especially CO<sub>2</sub><sup>+</sup> and O/C of 0.78 to 1.24, and a

128 nitrate inorganic aerosol (NIA) characterized by overwhelming  $\text{NO}^+$  and  $\text{NO}_2^+$ , as indicated in Fig S6. According to the  
129 diagnostic plots of the PMF analysis shown in Figure S2 to S4, the same organic factors as those in the traditional PMF analysis  
130 of only organic mass spectra were obtained. The  $\text{NO}^+$  and  $\text{NO}_2^+$  ions were distributed among different OA factors and the NIA  
131 factor; thus the concentrations of nitrate functionality ( $\text{NO}_{org}^+$  and  $\text{NO}_{2,org}^+$ ) in organic nitrates ( $\text{NO}_{3,org}$ ) are equal to the sum of  
132  $\text{NO}_2^+$  and  $\text{NO}^+$  via Eqs. (3) and (4), respectively (Xu et al., 2015b):

$$133 \quad \text{NO}_{2,org}^+ = \sum([\text{OA factor}]_i \times f_{\text{NO}_2,i}) \quad (3)$$

$$134 \quad \text{NO}_{org}^+ = \sum([\text{OA factor}]_i \times f_{\text{NO},i}) \quad (4)$$

135 where  $[\text{OA factor}]_i$  represents the mass concentration of OA factor  $i$ , and  $f_{\text{NO}_2,i}$  and  $f_{\text{NO},i}$  represent the mass fractions of  $\text{NO}_2^+$   
136 and  $\text{NO}^+$ , respectively.

137 It should be noted that the 4-factor solution seemed to have a “mixed factor” problem to some extent (Zhu et al., 2018). For  
138 example, HOA mixed with COA (clear  $\text{C}_3\text{H}_3\text{O}^+$  in  $m/z$  55 for spring, summer and autumn) (Mohr et al., 2012), and BBOA  
139 mixed with LO-OOA (clear  $m/z$  60 and 73 signals in LO-OOA in autumn) (Cubison et al., 2011). However, running PMF with  
140 more factors would produce unexplained factors but less influence on the apportionment of  $\text{NO}^+$  and  $\text{NO}_2^+$  ions between  
141 organic nitrates and inorganic nitrate (Table S1). In addition, the standard deviations of  $\text{NO}^+$  and  $\text{NO}_2^+$  ions in the OA factors  
142 across different FPEAK values (from  $-1.0$  to  $1.0$ ) were very small (Table S2). Therefore, the 4-factor solution was used for  
143 quantifying organic nitrates in spring, summer and autumn.

## 144 **3. Results and discussion**

### 145 **3.1 Organic nitrates estimation**

146 Table 2 shows the concentrations of nitrate functionality in organic nitrates (i.e.,  $\text{NO}_{3,org}$ ), estimated by both the  $\text{NO}^+/\text{NO}_2^+$   
147 ratio method and PMF method, as well as their contributions to the total measured nitrate. It should be noted that the small  
148 difference between the average  $R_{\text{obs}}$  and  $R_{\text{NH}_4\text{NO}_3}$  in winter leads to a large portion of negative data using the  $\text{NO}^+/\text{NO}_2^+$  ratio  
149 method (Table 1). The result from the PMF method shows that the contribution of organic nitrates in total nitrates is only 4.2%  
150 in winter (Figure S6), suggesting a negligible contribution of organic nitrates. Thus, we will only discuss organic nitrate  
151 estimation results in spring, summer and autumn. The analytical outcomes by the  $\text{NO}^+/\text{NO}_2^+$  ratio method and by the PMF  
152 method consistently suggest that organic nitrates had the highest ambient concentration ( $0.34\text{-}0.53 \mu\text{g m}^{-3}$ ) and proportion in  
153 total nitrates (41-64%) in summer among the different seasons. This finding agrees with the finding in (Ng et al., 2017) and it  
154 implies a seasonal trend in comparison with that of total nitrates in Table 1. Assuming the average molecular weight of organic  
155 nitrates of 200 to  $300 \text{ g mol}^{-1}$  (Rollins et al., 2012), we found that organic nitrates contributed 9-21% to OA in spring, 11-25%  
156 in summer, and 9-20% in autumn.

157 In the PMF method, the mass fractions of organic nitrates in HOA, LO-OOA and MO-OOA were 31%, 49% and 20%,  
158 respectively, in spring; 28%, 52% and 20%, respectively, in summer; 30%, 46% and 24%, respectively, in autumn. The major

159 fraction of organic nitrates occurring in LO-OOA for the three seasons implied that organic nitrates were mostly related to  
 160 fresher secondary OA formation. The NIA factors in all seasons were dominated by but are not limited to  $\text{NO}^+$  and  $\text{NO}_2^+$ .  
 161 Some organic fragments, such as  $\text{CO}_2^+$  and  $\text{C}_2\text{H}_3\text{O}^+$ , are also part of these factors, which agreed with the findings in the  
 162 literature (Hao et al., 2014; Xu et al., 2015b; Sun et al., 2012). This indicated the potential interference of organics in the NIA  
 163 factor. It is also worth to be noted that the  $\text{NO}^+/\text{NO}_2^+$  ratios in NIA (2.93 for spring, 3.53 for summer and 3.54 for autumn)  
 164 were higher than that for pure  $\text{NH}_4\text{NO}_3$  (Table 1), indicating an underestimation of  $\text{NO}_{3,\text{org}}$  concentration by the PMF method.  
 165 This finding may also explain the reason that the concentration of  $\text{NO}_{3,\text{org}}$  estimated using the PMF method was always close  
 166 to the lower estimation bound of  $\text{NO}_{3,\text{org}}$  concentration estimated using the  $\text{NO}^+/\text{NO}_2^+$  ratio method in each season (Table 2).

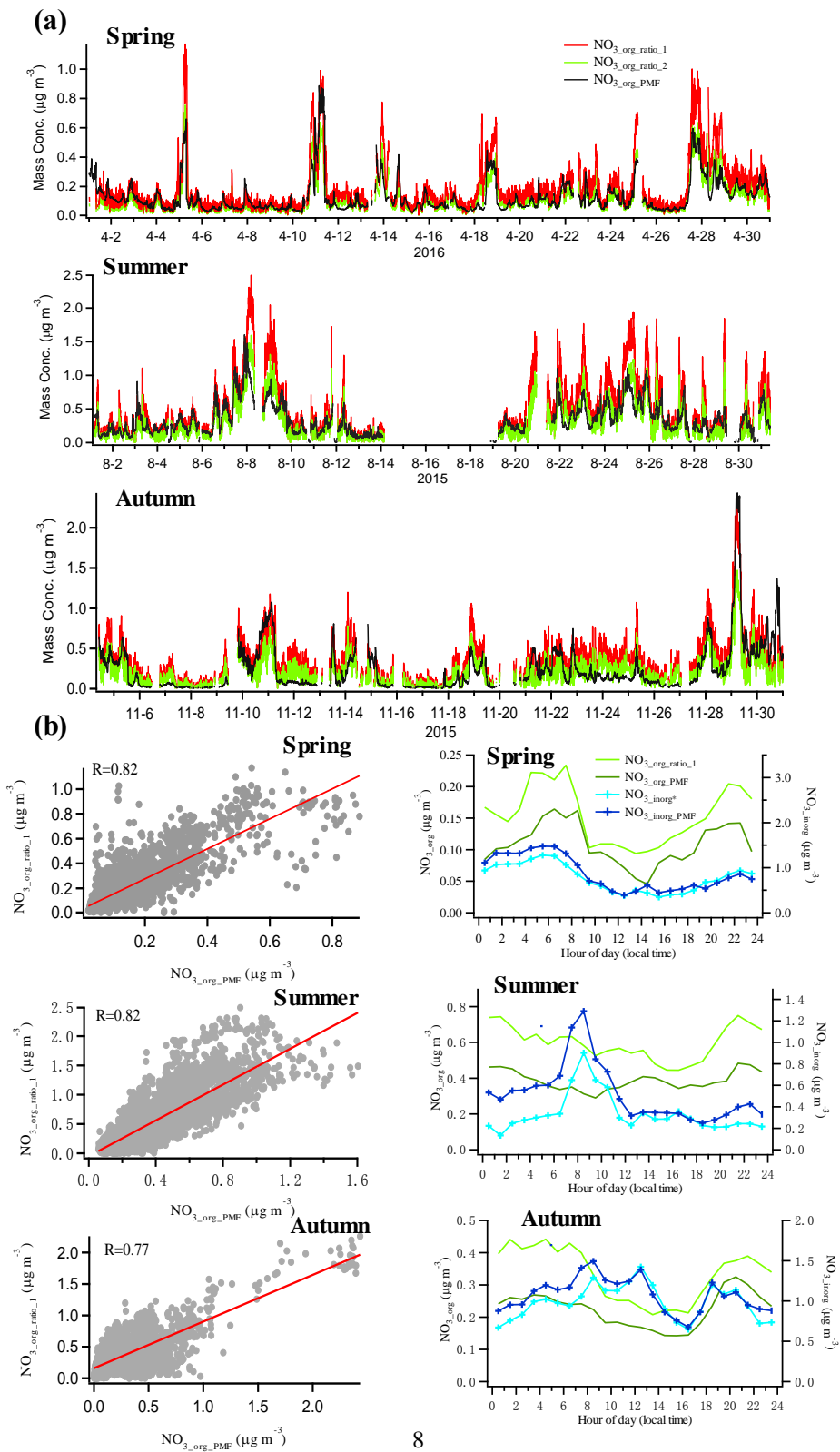
167 **Table 2.** Summary of organic nitrates estimations using the  $\text{NO}^+/\text{NO}_2^+$  ratio method and the PMF method

Sampling period	NO <sup>+</sup> /NO <sub>2</sub> <sup>+</sup> ratio method				PMF method	
	NO <sub>3,org</sub> (μg m <sup>-3</sup> ) <sup>a</sup>		NO <sub>3,org</sub> /NO <sub>3</sub>		NO <sub>3,org</sub> (μg m <sup>-3</sup> ) <sup>b</sup>	NO <sub>3,org</sub> /NO <sub>3</sub>
	lower	upper	lower	upper		
<b>Spring</b>	0.12	0.19	13%	21%	0.12	12%
<b>Summer</b>	0.34	0.53	41%	64%	0.39	43%
<b>Autumn</b>	0.21	0.33	16%	25%	0.21	16%
<b>Winter</b>	/	/	/	/	0.07	4.2%

168 <sup>a</sup> NO<sub>3,org</sub> for upper bound is denoted as NO<sub>3,org\_ratio\_1</sub>, and NO<sub>3,org</sub> for lower bound is denoted as NO<sub>3,org\_ratio\_2</sub>.

169 <sup>b</sup> NO<sub>3,org</sub> estimated using the PMF method is denoted as NO<sub>3,org\_PMF</sub>.

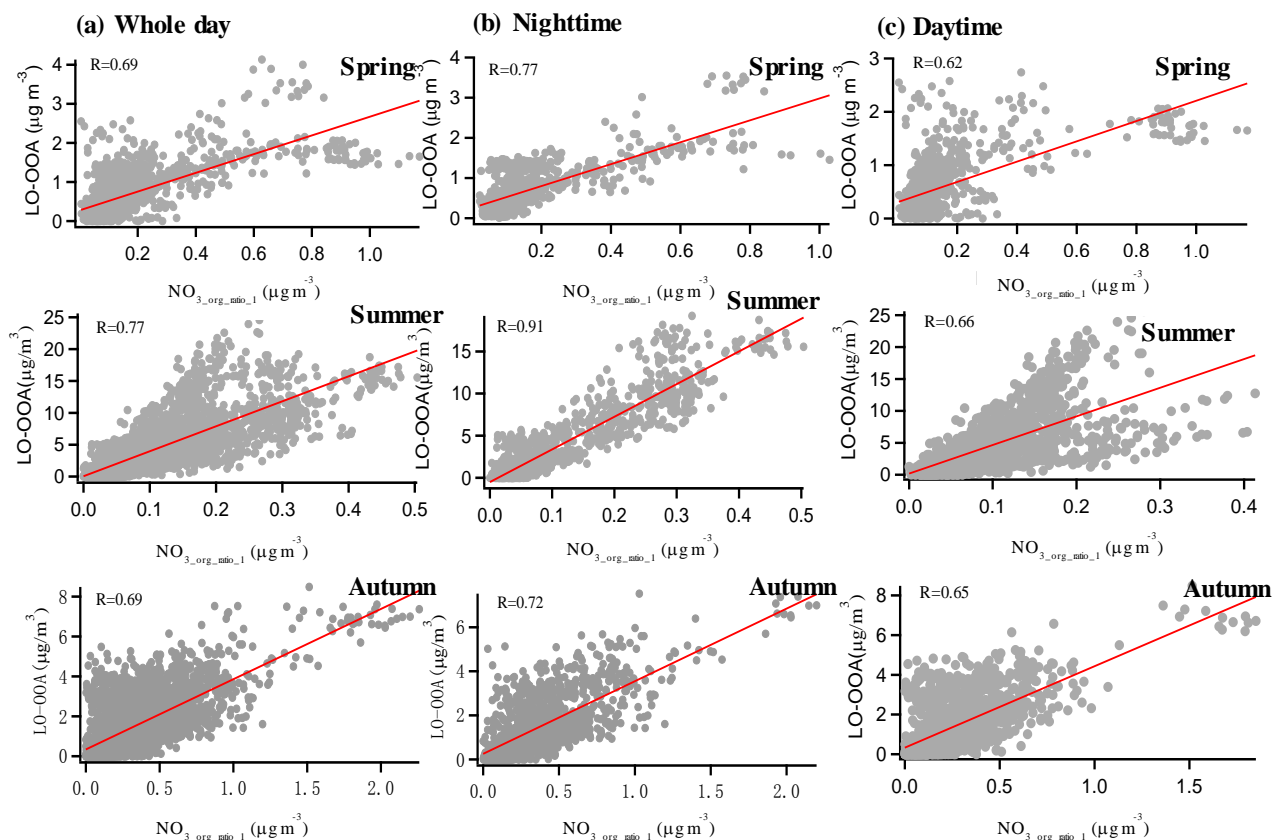
170 To further verify the reliability of the estimated results of organic nitrates, the NO<sub>3,org</sub> concentration time series calculated by  
 171 the two methods in each season are shown in Figure 2a. The computed correlation coefficients (R) are good (0.82 for spring,  
 172 0.82 for summer and 0.77 for autumn), indicating that similar results were achieved. The inorganic nitrate (NO<sub>3,inorg</sub>\*) obtained  
 173 by subtracting NO<sub>3,org\_ratio\_1</sub> from total measured nitrates also correlated well with the inorganic nitrate estimated using the  
 174 PMF method (R=0.92 for spring, 0.87 for summer and 0.86 for autumn). While they were distinctive from those of inorganic  
 175 nitrate (Figure 2b), which indicates that organic nitrates had been well separated from inorganic nitrate in this study, the diurnal  
 176 trends of organic nitrates obtained by the two methods were similar in each season, with lower concentrations in the daytime  
 177 and higher concentrations at night.



179 **Figure 2.** (a) Time series of  $\text{NO}_3\text{-org}$  concentration estimated by the  $\text{NO}^+/\text{NO}_2^+$  ratio method and PMF method for each  
 180 season; (b) correlations between  $\text{NO}_3\text{-org\_ratio\_1}$  and  $\text{NO}_3\text{-org\_PMF}$  (left panel); diurnal trends of organic nitrates and  $\text{NO}_3\text{-org}$   
 181 estimated by the different methods (right panel).

### 182 3.2 Correlation between organic nitrates and OA factors

183 As indicated by the results in the PMF method, the majority of organic nitrates were associated with LO-OOA in spring,  
 184 summer and autumn in the urban atmosphere in Shenzhen, implying a dominant secondary origin of organic nitrates. To further  
 185 confirm this relationship, we made the correlation analysis between organic nitrates estimated by the  $\text{NO}^+/\text{NO}_2^+$  ratio method  
 186 and the three factors resolved by the PMF analysis with only organic mass spectra in the three seasons. Generally, organic  
 187 nitrates were found better-correlated with LO-OOA ( $R=0.69\text{-}0.77$  in Figure 3) than with HOA and MO-OOA ( $R=0.03\text{-}0.69$  in  
 188 Figures S6-S8), which is consistent with the fact that the majority of organic nitrates were associated with LO-OOA in the  
 189 PMF method. However, the moderate correlation between organic nitrates and HOA implied possibility of direct emissions of  
 190 organic nitrates. Furthermore, we found a noticeably improved correlation between LO-OOA and organic nitrates at night  
 191 (19:00-6:00) and a reduced correlation during the daytime (7:00-18:00) in Figure 3, especially in summer, implying that  
 192 organic nitrates formation might be more closely related to secondary formation at night.

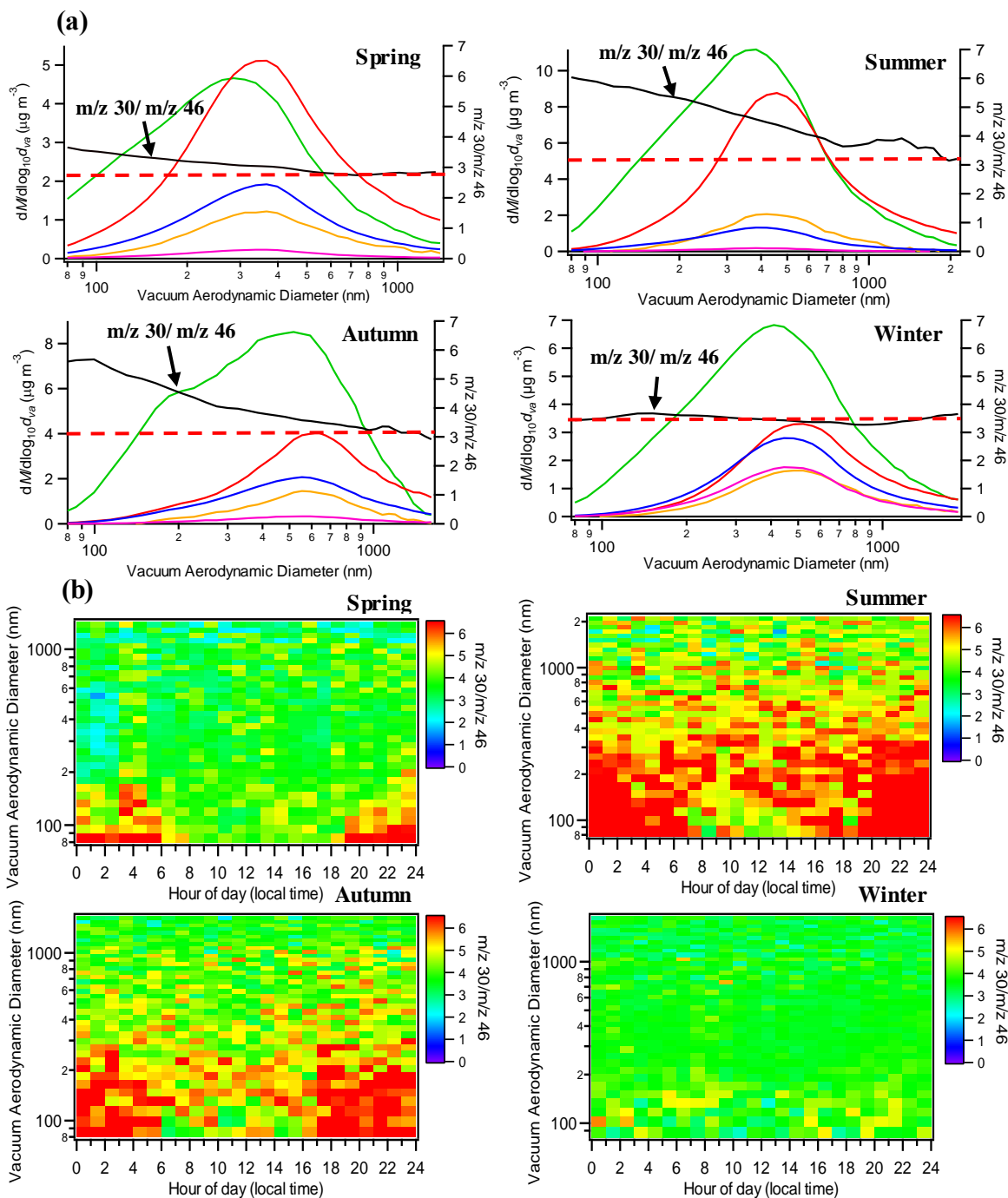


193

194 **Figure 3.**Correlation of  $\text{NO}_3\text{-org\_ratio}_1$  and LO-OOA in each season for the whole day (a), at night (b) and in the daytime (c).

### 195 3.3 Size distribution characteristics of organic nitrates

196 In this section, we attempt to use the  $\text{NO}^+/\text{NO}_2^+$  ratio as an indicator to investigate the size distribution characteristics of organic  
197 nitrates. Unfortunately, due to the lack of HR-PToF data, our analyses used the UMR-PToF data of  $m/z$  30 and 46, which  
198 might contain the interferences of  $\text{CH}_2\text{O}_x^+$  (Fry et al., 2018). In our case, the time variations of contributions of  $\text{CH}_2\text{O}^+$  in  $m/z$   
199 30 and  $\text{CH}_2\text{O}_2^+$  in  $m/z$  46 in the HR data of  $\text{PM}_{10}$  for the four seasons are shown in Figure S10. For all the four seasons, the  
200 average contributions of  $\text{CH}_2\text{O}_x^+$  in  $m/z$  30 and 46 in the HR data of  $\text{PM}_{10}$  were less than 10%, suggesting that the  $m/z$  30/ $m/z$   
201 46 ratio could mostly represent the  $\text{NO}^+/\text{NO}_2^+$  ratio. The average size distributions of  $m/z$  30 and  $m/z$  46 for the four seasons  
202 are shown in Figure S11, and Figure 4a shows the average size distributions of different aerosol species and the  $m/z$  30/ $m/z$  46  
203 ratio in the four seasons. It is clearly found that the  $m/z$  30/ $m/z$  46 ratio exhibited a decreasing trend in spring, summer and  
204 autumn, while it kept constant in winter, similar to the value of  $R_{\text{NH}_4\text{NO}_3}$  (red dotted line in Figure 4a). In addition, in spring,  
205 summer and autumn, the lowest values of the  $m/z$  30/ $m/z$  46 ratio, occurring at  $\sim 1 \mu\text{m}$ , were approximate to the corresponding  
206 seasonal values of  $R_{\text{NH}_4\text{NO}_3}$ . It should be noted that the similar size distribution patterns of the  $m/z$  30/ $m/z$  46 ratio under the  
207 highest interferences ( $>15\%$ ) and lowest interferences ( $<5\%$ ) of  $\text{CH}_2\text{O}_x^+$ , indicated by the HR data of  $\text{PM}_{10}$ , for spring, summer  
208 and autumn (Figure S12) imply that the size distribution patterns of the  $m/z$  30/ $m/z$  46 ratio were not affected significantly by  
209 the interferences of  $\text{CH}_2\text{O}_x^+$ . We also used the size distributions of the  $m/z$  30/ $m/z$  46 ratio to separate the size distributions of  
210 inorganic and organic nitrates, as shown in Figure S13, and the results indicate that organic nitrates were relatively more  
211 concentrated at small sizes compared to inorganic nitrates. Furthermore, the diurnal trends of the size distribution of the  $m/z$   
212 30/ $m/z$  46 ratio in spring, summer and autumn in Figure 4b show apparent higher values at small sizes at night, suggesting an  
213 important nighttime local origin of organic nitrates. Combining with the analysis in section 3.2, the local nighttime secondary  
214 formation of organic nitrates in warmer seasons in the urban polluted atmosphere in Shenzhen is highlighted. This is consistent  
215 with the previous findings in the US and Europe that the nighttime  $\text{NO}_3+\text{VOCs}$  reactions serve as an important source for  
216 particulate organic nitrates (Rollins et al., 2012; Xu et al., 2015a, 2015b; Fry et al., 2013; Lee et al., 2016). We will then  
217 explore the nighttime  $\text{NO}_3+\text{VOCs}$  reactions in Shenzhen in more detail in the following section.



218

219

220

**Figure 4.**(a) Average size distributions of aerosol species and m/z 30/m/z 46 ratio (red dotted line represents  $R_{\text{NH}_4\text{NO}_3}$ ); (b) diurnal trends of size distribution of m/z 30/m/z 46 ratio.

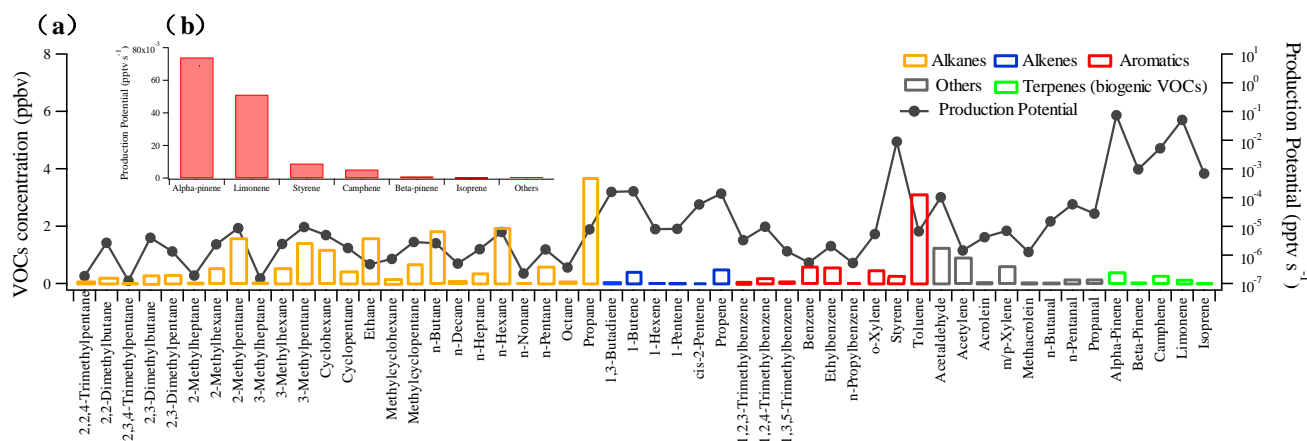
### 221 3.4 Nighttime particulate organic nitrates formation via NO<sub>3</sub>+VOCs

222 Since on-line VOCs measurement was only performed during the spring campaign (described in section 2.2), the following  
 223 theoretical analysis of NO<sub>3</sub>+VOCs reactions applies only to the spring case. NO<sub>3</sub>+VOCs reactions would yield a large mass of  
 224 gas- and particle-phase organic nitrates (Rollins et al., 2012; Nah et al., 2016; Boyd et al., 2015, 2017; Xu et al., 2015a, 2015b;  
 225 Lee et al., 2016). We used Eq. (9) to roughly judge the production potential (PP) of organic nitrates from a NO<sub>3</sub>+VOC reaction:

$$226 \quad [\text{Production Potential}]_{\text{NO}_3+\text{VOC}_i} = K_i \cdot [\text{VOC}_i] \cdot [\text{NO}_3] \quad (9)$$

227 Where  $K_i$  represents the reaction rate coefficient for NO<sub>3</sub> radical and a VOC;  $[\text{VOC}_i]$  is the concentration of the specific VOC;  
 228  $[\text{NO}_3]$  is the concentration of NO<sub>3</sub> radical. It should be noted that no organic nitrates yield parameter was introduced in Eq.  
 229 (9), because only a few organic nitrate yields for BVOCs were available in the literature (Fry et al., 2014; Ng et al., 2017).  
 230 However, given the fact that the values of  $K_i \cdot [\text{VOC}_i] \cdot [\text{NO}_3]$  for different VOC species can differ by orders of magnitude, not  
 231 multiplying the organic nitrate yields (ranging from 0 to 1) would not significantly affect the PP ranking of VOCs. In the spring  
 232 campaign, the diurnal variations of NO<sub>2</sub>, O<sub>3</sub> and estimated NO<sub>3</sub> radical concentrations are shown in Figure S14. It was found  
 233 that as a comparison to the nighttime NO<sub>3</sub> radical concentration reported in literature in the United States (Rollins et al., 2012;  
 234 Xu et al., 2015a), high concentration of NO<sub>2</sub> ( $19.93 \pm 2.31$  ppb) at night led to high yield of NO<sub>3</sub> radical ( $1.24 \pm 0.76$  ppt)  
 235 in Shenzhen, as calculated in Text S1.

236 The reaction rate coefficients of typical measured nighttime VOC concentrations with NO<sub>3</sub> radical and the production  
 237 potentials are listed in Table S3 and shown in Figure 5. These VOCs were considered based on their higher ambient  
 238 concentrations and availability for reaction kinetics with NO<sub>3</sub> radical. According to the distribution of production potential,  
 239 five biogenic VOCs (BVOCs) (i.e.,  $\alpha$ -pinene, limonene, camphene,  $\beta$ -pinene and isoprene) and one anthropogenic VOC  
 240 (styrene) were identified as notable VOC precursors with high production potential, while the sum of production potential  
 241 from the other VOCs was negligible as shown in Figure 5b.



242 **Figure 5.** (a) Mean concentrations of VOCs and the corresponding calculated production potential of NO<sub>3</sub>+VOC at night  
 243 during the spring campaign; (b) production potential ranking of VOCs at night during the spring campaign.  
 244

245 Based on the production potential evaluation above, we further explore SOA yield of NO<sub>3</sub>+the six notable VOC precursors  
 246 according to the analysis method of particulate organic nitrate formation in Xu et al. (2015a). Briefly, NO<sub>3</sub> and ozone are two  
 247 main oxidants for SOA formation from VOCs at night. Based on the concentrations of oxidants and the reaction rate constants  
 248 for VOCs with NO<sub>3</sub> and ozone, the branching ratio of each VOC that reacts with NO<sub>3</sub> can be estimated as in Eq. (10). By  
 249 combining the estimated branching ratios and SOA yields from chamber studies (Table 3, where the chamber conditions to  
 250 obtain the yields covered the range of aerosol mass loading in the spring campaign), potential SOA production from these  
 251 VOCs can be calculated as in Eq. (11) (Xu et al., 2015a):

$$252 \text{ branching ratio}_{\text{species } i+\text{NO}_3} = \frac{k_{[\text{species } i+\text{NO}_3] \times [\text{NO}_3]}}{k_{[\text{species } i+\text{NO}_3] \times [\text{NO}_3]} + k_{[\text{species } i+\text{O}_3] \times [\text{O}_3]}} \quad (10)$$

$$253 [\text{SOA}]_{\text{species,oxidant}} = [\text{species}] \times \text{branching ratio}_{\text{species,oxidant}} \times \text{yield}_{\text{species,oxidant}} \quad (11)$$

254 The results in Table 3 show that all six notable VOC species were prone to react with NO<sub>3</sub> radical instead of O<sub>3</sub> at night, and  
 255 the estimated potential SOA production from NO<sub>3</sub>+VOCs reactions using SOA mass yields in the literature was 0-0.33 μg m<sup>-3</sup>  
 256 for α-pinene, 0.09-1.28 μg m<sup>-3</sup> for limonene, 0.24 μg m<sup>-3</sup> for styrene, 0.004-0.06 μg m<sup>-3</sup> for β-pinene and 0.002-0.02 μg m<sup>-3</sup>  
 257 for isoprene. The SOA yield from camphene is currently unknown in the literature. It is seen that the average observed  
 258 nighttime concentration of particulate organic nitrates during the spring campaign (0.39-0.83 μg m<sup>-3</sup>, converting NO<sub>3,org\_ratio\_1</sub>,  
 259 NO<sub>3,org\_PMF</sub> in Figure 6 into organic nitrates assuming the average molecular weight of organic nitrates of 200 to 300 g mol<sup>-1</sup>)  
 260 was well within the estimated SOA concentration ranges produced by α-pinene, limonene and styrene in Table 3, indicating  
 261 that these three VOCs were the key VOC precursors in urban atmosphere in Shenzhen. Considering both the production  
 262 potentials and SOA yields, the contributions of β-pinene and isoprene to nighttime formation of particulate organic nitrates  
 263 could be negligible.

264 **Table 3.** Average concentrations, reaction branching and SOA production of α-pinene, limonene, styrene, camphene, β-  
 265 pinene and isoprene with respect to different oxidants at night in the spring campaign.

Species	Concentration (ppbv)	Rate coefficient <sup>a</sup>		Branching ratio		SOA yield from the literature (with NO <sub>3</sub> )	SOA from VOCs + NO <sub>3</sub> (μg m <sup>-3</sup> )
		NO <sub>3</sub>	O <sub>3</sub>	NO <sub>3</sub>	O <sub>3</sub>		
<b>α-pinene</b>	0.39	6.64E-12	7.2E-17	0.962	0.038	0-0.16 <sup>b</sup>	0-0.33
<b>Limonene</b>	0.14	1.22E-11	1.54E-16	0.957	0.043	0.12-1.74 <sup>c</sup>	0.09-1.28
<b>Styrene</b>	0.19	1.50E-12	1.70E-17	0.941	0.059	0.23 <sup>d</sup>	0.24
<b>Camphene</b>	0.28	6.20E-13	9.0E-19	0.992	0.008	/	/
<b>β-pinene</b>	0.01	2.51E-12	1.50E-17	0.968	0.032	0.07-1.04 <sup>e</sup>	0.004-0.06
<b>Isoprene</b>	0.032	6.96E-13	1.27E-17	0.908	0.091	0.02-0.24 <sup>f</sup>	0.002-0.02

266 <sup>a</sup> Rate coefficients for all species except camphene are from the MasterChemical Mechanism model  
267 (<http://mcm.leeds.ac.uk/MCM/>; under 25 °C), rate coefficients for camphene are from Martínez et al. (1999) and Atkinson et  
268 al. (1990).

269 <sup>b</sup> Hallquist et al. (1999); Spittler et al. (2006); Perraud et al. (2010); Fry et al. (2014).

270 <sup>c</sup> Fry et al. (2011, 2014); Spittler et al. (2006); Boyd et al. (2017).

271 <sup>d</sup> Cabrera-Perez et al. (2017).

272 <sup>e</sup> Griffin et al. (1999); Fry et al. (2009); Fry et al. (2014); Boyd et al. (2015).

273 <sup>f</sup> Rollins et al. (2009); Ng et al. (2008).

274 The estimation of potential SOA production above suggests significant contributions of  $\alpha$ -pinene, limonene, and styrene to  
275 SOA, and the significant contribution of camphene is also possible. Thus, we further explore the diurnal variations of the PPs  
276 of these four VOCs. Figure 6 shows the diurnal trends of BC, LO-OOA,  $\text{NO}_{3,\text{org\_ratio\_1}}$ ,  $\text{NO}_{3,\text{org\_PMF}}$ , and the PPs of the four  
277 VOCs during the spring campaign. There were two apparent nighttime growth periods (i.e., I: 19:00–22:00 and II: 2:00–6:00)  
278 for both  $\text{NO}_{3,\text{org\_ratio\_1}}$  and  $\text{NO}_{3,\text{org\_PMF}}$ . During Period I, BC maintained a relatively higher level, suggesting stable anthropogenic  
279 emissions. In contrast, the increases of all the PPs during Period I indicated that these precursors contributed to the organic  
280 nitrate growth. After 22:00, while the PPs still showed a rapid growth, BC and organic nitrates began to decrease, implying  
281 possible existence of other important anthropogenic VOC precursors, which were not identified by the GC-FID/MS analysis  
282 but would dominate the formation of organic nitrates at this stage. During Period II, the anthropogenic emissions remained at  
283 a stable lower level, as indicated by BC, while all the PPs increased with organic nitrates again, indicating that these four  
284 precursors also contributed to, or could dominate, this organic nitrate growth. As shown in Figure S15, organic nitrates  
285 correlated better with the PPs ( $R=0.63\text{--}0.74$ ) than with LO-OOA ( $R=0.19\text{--}0.31$ ) or BC ( $R=0.02\text{--}0.05$ ) during Period II at the  
286 spring campaign, suggesting the significant contributions of the  $\text{NO}_3$  reactions with these precursors.

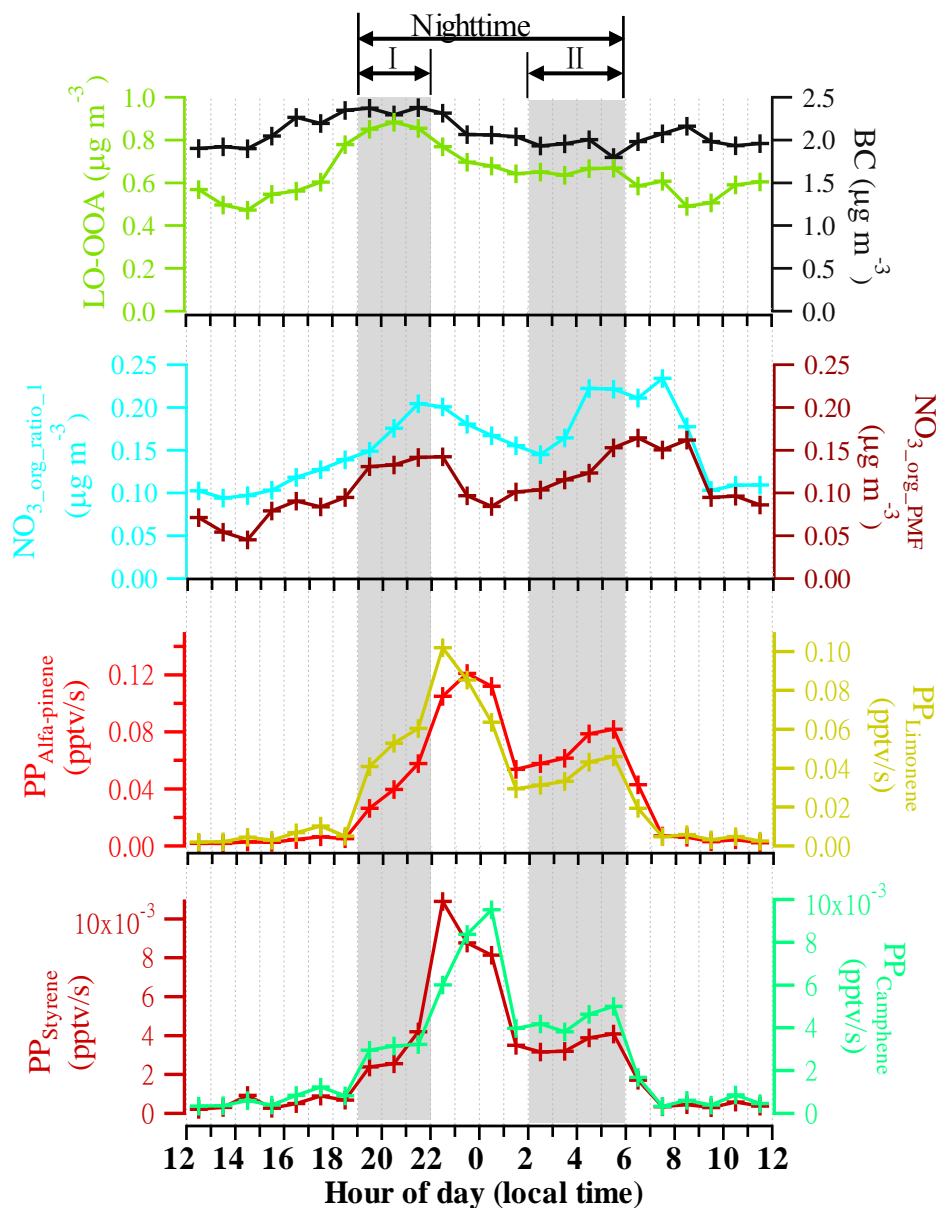


**Figure 6.** Diurnal trends of BC, LO-OOA,  $\text{NO}_3\text{.org\_ratio\_1}$ ,  $\text{NO}_3\text{.org\_PMF}$  and production potential (PP) of  $\alpha$ -pinene, limonene, styrene, and camphene during the spring campaign.

It should be noted that, all previous studies on nighttime organic nitrates formation in the US and Europe focused on mechanisms of  $\text{NO}_3$  reactions with BVOCs (Hallquist et al., 1999; Spittler et al., 2006; Perraud et al., 2010; Fry et al., 2014; Nah et al., 2016; Boyd et al., 2015, 2017). In this study, however, we found that anthropogenic VOCs could also play significant roles in particulate organic nitrate formation at night. Besides styrene, one of major aromatics (Cabrera-Perez et al., 2016), there were also other important anthropogenic VOC precursors that we did not identify in the spring campaign. In China,

295 styrene has been actually identified as an important VOC of non-methane hydrocarbons (NMHCs) in urban areas, and has a  
296 notable contribution to ozone formation and SOA production (An et al., 2009; Yuan et al., 2013; Zhu et al., 2019). This study  
297 highlights the possible key roles of anthropogenic VOC precursors in nighttime particulate organic nitrate formation in urban  
298 atmosphere in China, and relevant smog chamber studies for anthropogenic VOCs+NO<sub>3</sub> reactions are needed to support  
299 parameterization in modeling.

### 300 **3.5 Comparison with other similar studies and implications**

301 Table 4 shows the average ambient temperatures, average concentrations of NO, NO<sub>2</sub>, monoterpenes, NO<sub>3,org</sub>, the ratio of  
302 NO<sub>3,org</sub> to NO<sub>3,total</sub> and the ratio of organic nitrates to total organics in several similar field campaigns available in the literature,  
303 which implies the key role of NO<sub>3</sub>+VOCs reactions for nighttime particulate organic nitrate formation. In general, the variation  
304 of the particulate organic nitrates concentration is within an order of magnitude (0.06-0.98 μg/m<sup>3</sup>) among the different sites.  
305 Higher concentrations of particulate organic nitrates generally are associated with higher NO<sub>x</sub> concentrations rather than  
306 BVOC concentrations. On the other hand, although the BVOCs concentrations in Bakersfield were far less than that in other  
307 campaigns, the concentration of particulate organic nitrates there showed an intermediate level among all the campaigns.  
308 Therefore, it is suggested that the formation of particulate organic nitrates may be more relevant with NO<sub>x</sub> than BVOCs, which  
309 is consistent with the finding that the organic nitrate production was dominated by NO<sub>x</sub> in the southeastern US (Edwards et  
310 al., 2017). In the spring campaign of this study, we examined the correlation between organic nitrates and NO<sub>2</sub> or VOCs (by  
311 the sum of α pinene, limonene, camphene and styrene) at night (Figure S16) and found a significant correlation of organic  
312 nitrates with NO<sub>2</sub> (R=0.40-0.47) rather than with VOCs (R=0.22-0.23), which further suggests that the organic nitrates  
313 formation was driven by the NO<sub>x</sub>-involved NO<sub>3</sub> chemistry.

314

315 **Table 4.** Average ambient temperatures, average concentrations of monoterpenes,  $\text{NO}_{3,\text{total}}$ ,  $\text{NO}_{3,\text{org}}$ ,  $\text{NO}_{3,\text{org}}/\text{NO}_{3,\text{total}}$  and the ratio of organic nitrates to total organics (ON/Org) for different  
 316 field campaigns around the world. The ON results at the European and US sites are from Kiendler-Scharr et al. (2016) and Ng et al. (2017).

Sampling site	Site type	Sampling period	Temperature (°C)	NO (ppbv)	NO <sub>2</sub> (ppbv)	Monoterpenes (ppbv)	NO <sub>3,org</sub> (µg m <sup>-3</sup> )	NO <sub>3,org</sub> /NO <sub>3,total</sub>	ON/Org	Reference/Note
Bakersfield, US	rural	May-June, 2010	23.0		8.2	0.045 ( $\alpha$ -pinene) 0.004 ( $\beta$ -pinene) 0.034 (limonene)	0.16	0.28	0.23	Rollins et al. (2012)/ NO <sub>3,org</sub> measured by TD-LIF
Woodland Park, US	high attitude	July-August, 2011	15.0		1.2	0.25 (monoterpene)	0.06	0.86	0.09	Fry et al. (2013)/ Use AMS data to estimate NO <sub>3,org</sub>
Centreville, US	rural	June-July, 2013	24.7	0.1	1.1	0.350 ( $\alpha$ -pinene)* 0.312 ( $\beta$ -pinene)* 0.050 (limonene)*	0.08	1.00	0.10	Xu et al. (2015a)  Xu et al. (2015b)/ Use AMS data to estimate NO <sub>3,org</sub>
Barcelona, Spain	urban	March, 2009	13.3	11.0	23.6	0.423 (monoterpene)	0.48	0.13	0.13	Mohr et al. (2012)  Pandolfi et al. (2014) / Use AMS data to estimate NO <sub>3,org</sub>
Shenzhen, China	urban	April, 2016	24.5	8.0	19.4	0.391 ( $\alpha$ -pinene)* 0.013 ( $\beta$ -pinene)* 0.137 (limonene)*	0.16	0.17	0.11	This study/ Use AMS data to estimate NO <sub>3,org</sub>

317 \*BVOC concentration at night.

#### 318 4. Conclusions

319 An Aerodyne HR-ToF-AMS was deployed in urban Shenzhen for about one month per season during 2015–2016 to  
320 characterize particulate organic nitrates with high time resolution. We discovered high mass fractions of organic nitrates in  
321 total organics during warmer seasons, including spring (9-21%), summer (11-25%) and autumn (9-20%), while particulate  
322 organic nitrates were negligible in winter. The correlation analysis between organic nitrates and each OA factor showed high  
323 correlation ( $R=0.77$  in spring,  $0.91$  in summer and  $0.72$  in autumn) between organic nitrates and LO-OOA at night. The diurnal  
324 trend analysis of size distribution of  $m/z$  30/ $m/z$  46 ratio further suggested that organic nitrates formation mainly occurred at  
325 night. It also suggested that organic nitrates concentrated at smaller sizes, indicating that they were mostly local products. The  
326 calculated theoretical nighttime production potential of  $\text{NO}_3$  reacting with VOCs measured in spring showed that six VOC  
327 species (i.e.,  $\alpha$ -pinene, limonene, styrene, camphene,  $\beta$ -pinene and isoprene) were prominent precursors. The SOA yield  
328 analysis and the nighttime variation of production potential further indicated that  $\alpha$ -pinene, limonene, camphene and styrene  
329 could contribute significantly to nighttime formation of particulate organic nitrates in spring in Shenzhen, highlighting the  
330 unique contribution of anthropogenic VOCs as a comparison to that documented in previous studies in the US and Europe.  
331 Finally, the comparison of the results in this study with other similar studies implied that nighttime formation of particulate  
332 organic nitrates is more relevant with  $\text{NO}_x$  levels.

#### 333 Author contributions.

334 Xiao-Feng Huang designed the research. Kuangyou Yu and Qiao Zhu conducted data analysis and wrote the paper. Ke Du  
335 contributed to modelling and writing.

#### 336 Acknowledgments

337 This work was supported by National Key R&D Program of China (2018YFC0213901), National Natural Science Foundation  
338 of China (91544215; 41622304) and Science and Technology Plan of Shenzhen Municipality (JCYJ20170412150626172).

#### 339 References

- 340 An, J. L., Wang, Y. S., Sun, Y.: Effects of nonmethane hydrocarbons on ozone formation in Beijing. *Ecology & Environmental*  
341 *Sciences*.
- 342 Atkinson, R., Aschmann, S. M., Arey, J.: Rate constants for the gas-phase reactions of OH and  $\text{NO}_3$  radicals and  $\text{O}_3$  with  
343 sabinene and camphene at  $296 \pm 2$  K. *Atmospheric Environment. Part A. General Topics*, 24, (10), 2647-2654,  
344 [https://doi.org/10.1016/0960-1686\(90\)90144-C](https://doi.org/10.1016/0960-1686(90)90144-C), 1990

345 Ayres, B.R., Allen, H.M., Draper, D.C., Brown, S.S., Wild, R.J., Jimenez, J.L., Day, D.A., Campuzano-Jost, P., Hu, W., De  
346 Gouw, J.A., Koss, A., Cohen, R.C., Duffey, K.C., Romer, P., Baumann, K., Edgerton, E., Takahama, S., Thornton, J.A.,  
347 Lee, B.H., Lopez-Hilfiker, F.D., Mohr, C., Wennberg, P.O., Nguyen, T.B., Teng, A.P., Goldstein, A.H., Olson, K., Fry,  
348 J.L.: Organic nitrate aerosol formation via NO<sub>3</sub><sup>+</sup> biogenic volatile organic compounds in the southeastern United States.  
349 *Atmos. Chem. Phys.* 15, 13377-13392. <https://doi.org/10.5194/acp-15-13377-2015>, 2015.

350 Boyd, C.M., Nah, T., Xu, L., Berkemeier, T., Ng, N.L.: Secondary Organic Aerosol(SOA) from Nitrate Radical Oxidation of  
351 Monoterpenes: Effects of Temperature, Dilution, and Humidity on Aerosol Formation, Mixing, and Evaporation. *Environ.*  
352 *Sci. Technol.* 51, 7831–7841. <https://doi.org/10.1021/acs.est.7b01460>, 2017.

353 Boyd, C.M., Sanchez, J., Xu, L., Eugene, A.J., Nah, T., Tuet, W.Y., Guzman, M.I., Ng, N.L.: Secondary organic aerosol  
354 formation from the β-pinene+NO<sub>3</sub> system: effect of humidity and peroxy radical fate. *Atmos. Chem. Phys.* 15, 7497-  
355 7522. <https://doi.org/10.5194/acp-15-7497-2015>, 2015.

356 Bruns, E.A., Perraud, V., Zelenyuk, A., Ezell, M.J., Johnson, S.N., Yu, Y., Imre, D., Finlayson-Pitts, B.J., Alexander, M.L.:  
357 Comparison of FTIR and particle mass spectrometry for the measurement of particulate organic nitrates. *Environ. Sci.*  
358 *Technol.* 44, 1056-1061. <https://doi.org/10.1021/es9029864>, 2010.

359 Cabrera-Perez, D., Taraborrelli, D., Sander, R., and Pozzer, A.: Global atmospheric budget of simple monocyclic aromatic  
360 compounds, *Atmos. Chem. Phys.*, 16, 6931-6947, <https://doi.org/10.5194/acp-16-6931-2016>, 2016.

361 Cabrera-Perez, D., Taraborrelli, D., Lelieveld, J., Hoffmann, T., and Pozzer, A.: Global impact of monocyclic aromatics on  
362 tropospheric composition, *Atmos. Chem. Phys. Discuss.*, <https://doi.org/10.5194/acp-2017-928>, 2017.

363 Canagaratna, M.R., Jayne, J.T., Jimenez, J.L., Allan, J.D., Alfarra, M.R., Zhang, Q., Onasch, T.B., Drewnick, F., Coe, H.,  
364 Middlebrook, A., Delia, A., Williams, L.R., Trimborn, A.M., Northway, M.J., DeCarlo, P.F., Kolb, C.E., Davidovits, P.,  
365 Worsnop, D.R.: Chemical and microphysical characterization of ambient aerosols with the aerodyne aerosol mass  
366 spectrometer. *Mass Spectrom. Rev.* 26, 185-222. <https://doi.org/10.1002/mas.20115>, 2007.

367 Cubison, M. J., Ortega, A. M., Hayes, P. L., Farmer, D. K., Day, D., Lechner, M. J., Brune, W. H., Apel, E., Diskin, G. S.,  
368 Fisher, J. A., Fuelberg, H. E., Hecobian, A., Knapp, D. J., Mikoviny, T., Riemer, D., Sachse, G. W., Sessions, W., Weber,  
369 R. J., Weinheimer, A. J., Wisthaler, A., and Jimenez, J. L.: Effects of aging on organic aerosol from open biomass burning  
370 smoke in aircraft and laboratory studies, *Atmos. Chem. Phys.*, 11, 12049-12064, [https://doi.org/10.5194/acp-11-12049-](https://doi.org/10.5194/acp-11-12049-2011)  
371 [2011](https://doi.org/10.5194/acp-11-12049-2011), 2011.

372 Day, D. A., Liu, S., Russell, L. M., and Ziemann, P. J.: Organonitrate group concentrations in submicron particles with high  
373 nitrate and organic fractions in coastal southern California, *Atmos. Environ.*, 44, 1970–1979,  
374 <https://doi.org/10.1016/j.atmosenv.2010.02.045>, 2010.

375 DeCarlo, P.F., Kimmel, J.R., Trimborn, A., Northway, M.J., Jayne, J.T., Aiken, A.C., Gonin, M., Fuhrer, K., Horvath, T.,  
376 Docherty, K.S., Worsnop, D.R., Jimenez, J.L.: Field-deployable, high-resolution, time-of-flight aerosol mass  
377 spectrometer. *Anal. Chem.* 78, 8281-8289. <https://doi.org/10.1021/ac061249n>, 2006.

378 Edwards, P. M.; Aikin, K. C.; Dube, W. P.; Fry, J. L.; Gilman, J. B.; de Gouw, J. A.; Graus, M. G.; Hanisco, T. F.; Holloway,  
379 J.; Hübler, G.; Kaiser, J.; Keutsch, F. N.; Lerner, B. M.; Neuman, J. A.; Parrish, D. D.; Peischl, J.; Pollack, I. B.;  
380 Ravishankara, A. R.; Roberts, J. M.; Ryerson, T. B.; Trainer, M.; Veres, P. R.; Wolfe, G. M.; Warneke, C.; Brown, S. S.:  
381 Transition from high- to low-NO<sub>x</sub> control of night-time oxidation in the southeastern US. *Nature Geoscienc*, 10, (7), 490-  
382 495. <https://doi.org/10.1038/ngeo2976>, 2017.

383 Farmer, D.K., Matsunaga, A., Docherty, K.S., Surratt, J.D., Seinfeld, J.H., Ziemann, P.J., Jimenez, J.L.: Response of an aerosol  
384 mass spectrometer to organonitrates and organosulfates and implications for atmospheric chemistry. *Proc. Natl. Acad.*  
385 *Sci.* 107, 6670-6675. <https://doi.org/10.1073/pnas.0912340107>, 2010.

386 Fry, J. L., Brown, S. S., Middlebrook, A. M., Edwards, P. M., Campuzano-Jost, P., Day, D. A., Jimenez, J. L., Allen, H. M.,  
387 Ryerson, T. B., Pollack, I., Graus, M., Warneke, C., de Gouw, J. A., Brock, C. A., Gilman, J., Lerner, B. M., Dubé, W.  
388 P., Liao, J., and Welti, A.: Secondary organic aerosol (SOA) yields from NO<sub>3</sub> radical + isoprene based on nighttime  
389 aircraft power plant plume transects, *Atmos. Chem. Phys.*, 18, 11663-11682, <https://doi.org/10.5194/acp-18-11663-2018>,  
390 2018.

391 Fry, J.L., Draper, D.C., Barsanti, K.C., Smith, J.N., Ortega, J., Winkler, P.M., Lawler, M.J., Brown, S.S., Edwards, P.M.,  
392 Cohen, R.C.: Secondary Organic Aerosol Formation and Organic Nitrate Yield from NO<sub>3</sub> Oxidation of Biogenic  
393 Hydrocarbons. *Environ. Sci. Technol.* 48, 11944–11953. <https://doi.org/10.1021/es502204x>, 2014.

394 Fry, J.L., Draper, D.C., Zarzana, K.J., Campuzano-Jost, P., Day, D.A., Jimenez, J.L., Brown, S.S., Cohen, R.C., Kaser, L.,  
395 Hansel, A., Cappellin, L., Karl, T., Hodzic Roux, A., Turnipseed, A., Cantrell, C., Lefer, B.L., Grossberg, N.:  
396 Observations of gas- and aerosol-phase organic nitrates at BEACHON-RoMBAS 2011. *Atmos. Chem. Phys.* 13, 8585-  
397 8605. <https://doi.org/10.5194/acp-13-8585-2013>, 2013.

398 Fry, J.L., Kiendler-Scharr, A., Rollins, A.W., Brauers, T., Brown, S.S., Dorn, H.P., Dubé, W.P., Fuchs, H., Mensah, A., Rohrer,  
399 F., Tillmann, R., Wahner, A., Wooldridge, P.J., Cohen, R. C.: SOA from limonene: Role of NO<sub>3</sub> in its generation and  
400 degradation. *Atmos. Chem. Phys.* 11, 3879-3894. <https://doi.org/10.5194/acp-11-3879-2011>, 2011.

401 Fry, J.L., Kiendlerscharr, A., Rollins, A.W., Wooldridge, P.J., Brown, S.S., Fuchs, H., Dube, W.P., Mensah, A., Dal Maso,  
402 M., Tillmann, R.: Organic nitrate and secondary organic aerosol yield from NO<sub>3</sub> oxidation of β-pinene evaluated using  
403 a gas-phase kinetics/aerosol partitioning model. *Atmos. Chem. Phys.* 9, 1431–1449. [https://doi.org/10.5194/acp-9-1431-](https://doi.org/10.5194/acp-9-1431-2009)  
404 [2009](https://doi.org/10.5194/acp-9-1431-2009), 2009.

405 Griffin, R. J., Cocker, D. R., III, Flagan, R. C., and Seinfeld, J. H.: Organic aerosol formation from the oxidation of biogenic  
406 hydrocarbons. *J. Geophys. Res.*, 104, 3555–3567, <https://doi.org/10.1029/1998jd100049>, 1999.

407 Hallquist, M., Wängberg, I., Ljungström, E., Barnes, I., Becker, K.H.: Aerosol and product yields from NO<sub>3</sub>radical-initiated  
408 oxidation of selected monoterpenes. *Environ. Sci. Technol.* 33, 553-559. <https://doi.org/10.1021/es980292s>, 1999.

409 Hao, L.Q., Kortelainen, A., Romakkaniemi, S., Portin, H., Jaatinen, A., Leskinen, A., Komppula, M., Miettinen, P., Sueper,  
410 D., Pajunoja, A., Smith, J.N., Lehtinen, K.E.J., Worsnop, D.R., Laaksonen, A., Virtanen, A.: Atmospheric submicron

411 aerosol composition and particulate organic nitrate formation in a boreal forestland-urban mixed region. *Atmos. Chem.*  
412 *Phys.* 14, 13483-13495. <https://doi.org/10.5194/acp-14-13483-2014>, 2014.

413 He, L.Y., Huang, X.F., Xue, L., Hu, M., Lin, Y., Zheng, J., Zhang, R., Zhang, Y.H.: Submicron aerosol analysis and organic  
414 source apportionment in an urban atmosphere in Pearl River Delta of China using high-resolution aerosol mass  
415 spectrometry. *J. Geophys. Res. Atmos.* 116, D12. <https://doi.org/10.1029/2010JD014566>, 2011.

416 Huang, X.F., He, L.Y., Hu, M., Canagaratna, M.R., Sun, Y., Zhang, Q., Zhu, T., Xue, L., Zeng, L.W., Liu, X.G., Zhang, Y.H.,  
417 Jayne, J.T., Ng, N.L., Worsnop, D.R.: Highly time-resolved chemical characterization of atmospheric submicron particles  
418 during 2008 Beijing Olympic games using an aerodyne high-resolution aerosol mass spectrometer. *Atmos. Chem. Phys.*  
419 10, 8933-8945. <https://doi.org/10.5194/acp-10-8933-2010>, 2010.

420 Huang, X.F., He, L.Y., Xue, L., Sun, T.L., Zeng, L.W., Gong, Z.H., Hu, M., Zhu, T.: Highly time-resolved chemical  
421 characterization of atmospheric fine particles during 2010 Shanghai World Expo. *Atmos. Chem. Phys.* 12, 4897-4907.  
422 <https://doi.org/10.5194/acp-12-4897-2012>, 2012.

423 Huang, X.F., Xue, L., Tian, X.D., Shao, W.W., Sun, T. Le, Gong, Z.H., Ju, W.W., Jiang, B., Hu, M., He, L.Y.: Highly time-  
424 resolved carbonaceous aerosol characterization in Yangtze River Delta of China: Composition, mixing state and  
425 secondary formation. *Atmos. Environ.* 64, 200-207. <https://doi.org/10.1016/j.atmosenv.2012.09.059>, 2013.

426 Jimenez, J. L., Jayne, J. T., Shi, Q., Kolb, C. E., Worsnop, D. R., Yourshaw, I., Seinfeld, J. H., Flagan, R. C., Zhang, X. F.,  
427 Smith, K. A., Morris, J. W., and Davidovits, P.: Ambient aerosol sampling using the aerodyne aerosol mass spectrometer,  
428 *J. Geophys. Res.-Atmos.*, 108, 447–457, <https://doi.org/10.1029/2001JD001213>, 2003.

429 Kiendler-Scharr, A., Mensah, A. A., Friese, E., Topping, D., Nemitz, E., Prevot, A. S. H., Äijälä, M., Allan, J., Canonaco, F.,  
430 Canagaratna, M., Carbone, S., Crippa, M., Dall'Osto, M., Day, D. A., De Carlo, P., Di Marco, C. F., Elbern, H., Eriksson,  
431 A., Freney, E., Hao, L., Herrmann, H., Hildebrandt, L., Hillamo, R., Jimenez, J. L., Laaksonen, A., McFiggans, G., Mohr,  
432 C., O'Dowd, C., Otjes, R., Ovadnevaite, J., Pandis, S. N., Poulain, L., Schlag, P., Sellegri, K., Swietlicki, E., Tiitta, P.,  
433 Vermeulen, A., Wahner, A., Worsnop, D., and Wu, H. C.: Organic nitrates from night-time chemistry are ubiquitous in  
434 the European submicron aerosol, *Geophys. Res. Lett.*, 43, 7735–7744, <https://doi.org/10.1002/2016GL069239>, 2016.

435 Lee, B.H., Mohr, C., Lopez-Hilfiker, F.D., Lutz, A., Hallquist, M., Lee, L., Romer, P., Cohen, R.C., Iyer, S., Kurten, T., Hu,  
436 W., Day, D.A., Campuzano-Jost, P., Jimenez, J.L., Xu, L., Ng, N.L., Guo, H., Weber, R.J., Wild, R.J., Brown, S.S., Koss,  
437 A., de Gouw, J., Olson, K., Goldstein, A.H., Seco, R., Kim, S., McAvey, K., Shepson, P.B., Starn, T., Baumann, K.,  
438 Edgerton, E.S., Liu, J., Shilling, J.E., Miller, D.O., Brune, W., Schobesberger, S., D'Ambro, E.L., Thornton, J.A.: Highly  
439 functionalized organic nitrates in the southeast United States: Contribution to secondary organic aerosol and reactive  
440 nitrogen budgets. *Proc. Natl. Acad. Sci.* 113, 1516-1521. <https://doi.org/10.1073/pnas.1508108113>, 2016.

441 Lelieveld, J., Gromov, S., Pozzer, A., Taraborrelli, D.: Global tropospheric hydroxyl distribution, budget and reactivity. *Atmos.*  
442 *Chem. Phys.* 16, 12477-12493. <https://doi.org/10.5194/acp-16-12477-2016>, 2016.

443 Martínez, E.; Cabañas, B.; Aranda, A.; Martín, P.; Salgado, S.: Absolute Rate Coefficients for the Gas-Phase Reactions of  
444 NO<sub>3</sub> Radical with a Series of Monoterpenes at T = 298 to 433 K. *Journal of Atmospheric Chemistry*, 33, (3), 265-282.  
445 <https://doi.org/10.1023/A:1006178530211>, 1999.

446 Middlebrook, A.M., Bahreini, R., Jimenez, J.L., Canagaratna, M.R.: Evaluation of composition-dependent collection  
447 efficiencies for the Aerodyne aerosol mass spectrometer using field data. *Aerosol Sci. Technol.* 46, 258-271.  
448 <https://doi.org/10.1080/02786826.2011.620041>, 2012.

449 Mohr, C., DeCarlo, P. F., Heringa, M. F., Chirico, R., Slowik, J. G., Richter, R., Reche, C., Alastuey, A., Querol, X., Seco, R.,  
450 Peñuelas, J., Jiménez, J. L., Crippa, M., Zimmermann, R., Baltensperger, U., and Prévôt, A. S. H.: Identification and  
451 quantification of organic aerosol from cooking and other sources in Barcelona using aerosol mass spectrometer data,  
452 *Atmos. Chem. Phys.*, 12, 1649–1665, <https://doi.org/10.5194/acp-12-1649-2012>, 2012.

453 Nah, T., Sanchez, J., Boyd, C. M., and Ng, N. L.: Photochemical Aging of  $\alpha$ -pinene and  $\beta$ -pinene Secondary Organic  
454 Aerosol formed from Nitrate Radical Oxidation, *Environ. Sci. Technol.*, 50, 222–231,  
455 <https://doi:10.1021/acs.est.5b04594>, 2016.

456 Ng, N. L., Brown, S. S., Archibald, A. T., Atlas, E., Cohen, R. C., Crowley, J. N., Day, D. A., Donahue, N. M., Fry, J. L.,  
457 Fuchs, H., Griffin, R. J., Guzman, M. I., Herrmann, H., Hodzic, A., Iinuma, Y., Jimenez, J. L., Kiendler-Scharr, A., Lee,  
458 B. H., Luecken, D. J., Mao, J., McLaren, R., Mutzel, A., Osthoff, H. D., Ouyang, B., Picquet-Varrault, B., Platt, U., Pye,  
459 H. O. T., Rudich, Y., Schwantes, R. H., Shiraiwa, M., Stutz, J., Thornton, J. A., Tilgner, A., Williams, B. J., and Zaveri,  
460 R. A.: Nitrate radicals and biogenic volatile organic compounds: oxidation, mechanisms, and organic aerosol, *Atmos.*  
461 *Chem. Phys.*, 17, 2103-2162, <https://doi.org/10.5194/acp-17-2103-2017>, 2017.

462 Ng, N. L., Canagaratna, M. R., Zhang, Q., Jimenez, J. L., Tian, J., Ulbrich, I. M., Kroll, J. H., Docherty, K.S., Chhabra, P.S.,  
463 Bahreini, R., Murphy, S.M., Seinfeld, J.H., Hildebrandt, L., Donahue, N.M., Decarlo, P.F., Lanz, V.A., Prévôt, A.S.H.,  
464 Dinar, E., Rudich, Y., Worsnop, D.R.: Organic aerosol components observed in Northern Hemispheric datasets from  
465 Aerosol Mass Spectrometry. *Atmos. Chem. Phys.* 10, 4625-4641. <https://doi.org/10.5194/acp-10-4625-2010>, 2010.

466 Ng, N. L., Kwan, A. J., Surratt, J. D., Chan, A. W. H., Chhabra, P. S., Sorooshian, A., Pye, H. O. T., Crounse, J. D., Wennberg,  
467 P. O., Flagan, R. C., and Seinfeld, J. H.: Secondary organic aerosol (SOA) formation from reaction of isoprene with  
468 nitrate radicals (NO<sub>3</sub>), *Atmos. Chem. Phys.*, 8, 4117–4140, <https://doi.org/10.5194/acp-8-4117-2008>, 2008.

469 Pandolfi, M.; Querol, X.; Alastuey, A.; Jimenez, J. L.; Jorba, O.; Day, D.; Ortega, A.; Cubison, M. J.; Comerón, A.; Sicard,  
470 M.; Mohr, C.; Prévôt, A. S. H.; Minguillón, M. C.; Pey, J.; Baldasano, J. M.; Burkhardt, J. F.; Seco, R.; Peñuelas, J.; van  
471 Drooge, B. L.; Artiñano, B.; Di Marco, C.; Nemitz, E.; Schallhart, S.; Metzger, A.; Hansel, A.; Lorente, J.; Ng, S.; Jayne,  
472 J.; Szidat, S.: Effects of sources and meteorology on particulate matter in the Western Mediterranean Basin: An overview  
473 of the DAURE campaign. *Journal of Geophysical Research: Atmospheres*, 119, (8), 4978-5010.  
474 <https://10.1002/2013JD021079>, 2014.

475 Perraud, V., Bruns, E. A., Ezell, M. J., Johnson, S. N., Greaves, J., and Finlayson-Pitts, B. J.: Identification of organic nitrates  
476 in the NO<sub>3</sub> radical initiated oxidation of  $\alpha$ -pinene by atmospheric pressure chemical ionization mass spectrometry,  
477 Environ. Sci. Technol., 44, 5887–5893. <https://doi.org/10.1021/es1005658>, 2010.

478 Rollins, A.W., Browne, E.C., Min, K.-E., Pusede, S.E., Wooldridge, P.J., Gentner, D.R., Goldstein, A.H., Liu, S., Day, D.A.,  
479 Russell, L.M., Cohen, R.C.: Evidence for NO<sub>x</sub> Control over Nighttime SOA Formation. Science. 337, 1210-1212.  
480 <https://doi.org/10.1126/science.1221520>, 2012.

481 Rollins, A. W., Kiendler-Scharr, A., Fry, J. L., Brauers, T., Brown, S. S., Dorn, H.-P., Dubé, W. P., Fuchs, H., Mensah, A.,  
482 Mentel, T. F., Rohrer, F., Tilmann, R., Wegener, R., Wooldridge, P. J., and Cohen, R. C.: Isoprene oxidation by nitrate  
483 radical: alkyl nitrate and secondary organic aerosol yields, Atmos. Chem. Phys., 9, 6685–6703,  
484 <https://doi.org/10.5194/acp-9-6685-2009>, 2009.

485 Sato, K., Takami, A., Isozaki, T., Hikida, T., Shimono, A., Imamura, T.: Mass spectrometric study of secondary organic aerosol  
486 formed from the photo-oxidation of aromatic hydrocarbons. Atmos. Environ. 44, 1080-1087.  
487 <https://doi.org/10.1016/j.atmosenv.2009.12.013>, 2010.

488 Sobanski, N., Thieser, J., Schuladen, J., Sauvage, C., Song, W., Williams, J., Lelieveld, J., Crowley, J.N.: Day and night-time  
489 formation of organic nitrates at a forested mountain site in south-west Germany. Atmos. Chem. Phys. 17, 4115-4130.  
490 <https://doi.org/10.5194/acp-17-4115-2017>, 2017.

491 Spittler, M., Barnes, I., Bejan, I., Brockmann, K.J., Benter, T., Wirtz, K.: Reactions of NO<sub>3</sub> radicals with limonene and  $\alpha$ -  
492 pinene : Product and SOA formation. Atmos. Environ. 40, 116–127. <https://doi.org/10.1016/j.atmosenv.2005.09.093>,  
493 2006.

494 Sun, Y., Zhang, Q., Schwab, J.J., Yang, T., Ng, N.L., Demerjian, K.L.: Factor analysis of combined organic and inorganic  
495 aerosol mass spectra from high resolution aerosol mass spectrometer measurements. Atmos. Chem. Phys. 12, 8537–8551.  
496 <https://doi.org/10.5194/acp-12-8537-2012>, 2012.

497 Teng, A.P., Crounse, J.D., Lee, L., St. Clair, J.M., Cohen, R.C., Wennberg, P.O.: Hydroxy nitrate production in the OH-  
498 initiated oxidation of alkenes. Atmos. Chem. Phys. 139, 5367-5377. <https://doi.org/10.5194/acp-15-4297-2015>, 2015.

499 Teng, A.P., Crounse, J.D., Wennberg, P.O.: Isoprene Peroxy Radical Dynamics. J. Am. Chem. Soc. 139, 4297-4316.  
500 <https://doi.org/10.1021/jacs.6b12838>, 2017.

501 Wang, H.; Lu, K.; Chen, X.; Zhu, Q.; Chen, Q.; Guo, S.; Jiang, M.; Li, X.; Shang, D.; Tan, Z.; Wu, Y.; Wu, Z.; Zou, Q.; Zheng,  
502 Y.; Zeng, L.; Zhu, T.; Hu, M.; Zhang, Y.: High N<sub>2</sub>O<sub>5</sub> Concentrations Observed in Urban Beijing: Implications of a Large  
503 Nitrate Formation Pathway. Environmental Science & Technology Letters, 4, (10), 416-420.  
504 <https://doi.10.1021/acs.estlett.7b00341>, 2018.

505 Wang, M.; Zeng, L.; Lu, S.; Shao, M.; Liu, X.; Yu, X.; Chen, W.; Yuan, B.; Zhang, Q.; Hu, M.; Zhang, Z.: Development and  
506 validation of a cryogen-free automatic gas chromatograph system (GC-MS/FID) for online measurements of volatile  
507 organic compounds, 6, (23), 9424-9434. Analytical Methods, <https://doi.10.1039/C4AY01855A>, 2014.

508 Xu, L., Guo, H., Boyd, C.M., Klein, M., Bougiatioti, A., Cerully, K.M., Hite, J.R., Isaacman-VanWertz, G., Kreisberg, N.M.,  
509 Knote, C., Olson, K., Koss, A., Goldstein, A.H., Hering, S. V., de Gouw, J., Baumann, K., Lee, S.-H., Nenes, A., Weber,  
510 R.J., Ng, N.L.: Effects of anthropogenic emissions on aerosol formation from isoprene and monoterpenes in the  
511 southeastern United States. *Proc. Natl. Acad. Sci.* 112, 37-42. <https://doi.org/10.1073/pnas.1417609112>, 2015a.

512 Xu, L., Suresh, S., Guo, H., Weber, R.J., Ng, N.L.: Aerosol characterization over the southeastern United States using high-  
513 resolution aerosol mass spectrometry: Spatial and seasonal variation of aerosol composition and sources with a focus on  
514 organic nitrates. *Atmos. Chem. Phys.* 15, 7307-7336. <https://doi.org/10.5194/acp-15-7307-2015>, 2015b.

515 Xu, W., Sun, Y., Wang, Q., Du, W., Zhao, J., Ge, X., Han, T., Zhang, Y., Zhou, W., Li, J., Fu, P., Wang, Z., Worsnop, D.R.:  
516 Seasonal Characterization of Organic Nitrogen in Atmospheric Aerosols Using High Resolution Aerosol Mass  
517 Spectrometry in Beijing, China. *ACS Earth Sp. Chem.* 1, 673–682. <https://doi.org/10.1021/acsearthspacechem.7b00106>,  
518 2017.

519 Yan, C., Nie, W., Äijälä, M., Rissanen, M.P., Canagaratna, M.R., Massoli, P., Junninen, H., Jokinen, T., Sarnela, N., Häme,  
520 S.A.K., Schobesberger, S., Canonaco, F., Yao, L., Prévôt, A.S.H., Petäjä, T., Kulmala, M., Sipilä, M., Worsnop, D.R.,  
521 Ehn, M.: Source characterization of highly oxidized multifunctional compounds in a boreal forest environment using  
522 positive matrix factorization. *Atmos. Chem. Phys.* 16, 12715-12731. <https://doi.org/10.5194/acp-16-12715-2016>, 2016.

523 Yuan, B., Hu, W. W., Shao, M., Wang, M., Chen, W. T., Lu, S. H., Zeng, L. M., and Hu, M.: VOC emissions, evolutions and  
524 contributions to SOA formation at a receptor site in eastern China, *Atmos. Chem. Phys.*, 13, 8815-8832,  
525 <https://doi.org/10.5194/acp-13-8815-2013>, 2013.

526 Zhang, Q., Jimenez, J.L., Canagaratna, M.R., Ulbrich, I.M., Ng, N.L., Worsnop, D.R., Sun, Y.: Understanding atmospheric  
527 organic aerosols via factor analysis of aerosol mass spectrometry: A review. *Anal. Bioanal. Chem.* 401, 3045-3067.  
528 <https://doi.org/10.1007/s00216-011-5355-y>, 2011.

529 Zhang, Y.H., Su, H., Zhong, L.J., Cheng, Y.F., Zeng, L.M., Wang, X.S., Xiang, Y.R., Wang, J.L., Gao, D.F., Shao, M., Fan,  
530 S.J., Liu, S.C.: Regional ozone pollution and observation-based approach for analyzing ozone-precursor relationship  
531 during the PRIDE-PRD2004 campaign. *Atmos. Environ.* 42, 6203-6218. <https://doi.org/10.1016/j.atmosenv.2008.05.002>,  
532 2008.

533 Zhu, B., Han, Y., Wang, C., Huang, X. F., Xia, S. Y., Niu, Y. B., Yin, Z. X, He, L.Y. :Understanding primary and secondary  
534 sources of ambient oxygenated volatile organic compounds in Shenzhen utilizing photochemical age-based  
535 parameterization method. *Journal of Environmental Sciences*, 75, 105-114. <https://doi.org/10.1016/j.jes.2018.03.008>,  
536 2019.

537 Zhu, Q., He, L.Y., Huang, X.F., Cao, L.M., Gong, Z.H., Wang, C., Zhuang, X., Hu, M.: Atmospheric aerosol compositions  
538 and sources at two national background sites in northern and southern China. *Atmos. Chem. Phys.* 16, 10283-10297.  
539 <https://doi.org/10.5194/acp-16-10283-2016>, 2016.

540 Zhu, Q., Huang, X.-F., Cao, L.-M., Wei, L.-T., Zhang, B., He, L.-Y., Elser, M., Canonaco, F., Slowik, J. G., Bozzetti, C., El-  
541 Haddad, I., and Prévôt, A. S. H.: Improved source apportionment of organic aerosols in complex urban air pollution using  
542 the multilinear engine (ME-2), *Atmos. Meas. Tech.*, 11, 1049-1060. <https://doi.org/10.5194/amt-11-1049-2018>, 2018.